Expansion of DUB functionality generated by alternative isoforms

Leznicki, Pawel; Natarajan, Jayaprakash; Bader, Gerd; Spevak, Walter; Schlattl, Andreas; Rehman, Syed Arif Abdul

Published in:
Journal of Cell Science

DOI:
10.1242/jcs.212753

Publication date:
2018

Document Version
Peer reviewed version

Expansion of DUB functionality by alternative isoforms: USP35, a case study

Pawel Leznicki[1,4,‡,*], Jayaprakash Natarajan[1,‡] , Gerd Bader[2], Walter Spevak[2], Andreas Schlattl[2], Syed Arif Abdul Rehman[1], Deepika Pathak, Simone Weidlich[1], Andreas Zoephel[2], Marie C Bordone[3], Nuno L Barbosa-Morais[3], Guido Boehmelt[2] and Yogesh Kulathu[1,*]

[1] MRC Protein Phosphorylation and Ubiquitylation Unit, School of Life Sciences, University of Dundee, Dundee, UK

[2] Boehringer Ingelheim RCV GmbH & Co KG, Dr. Boehringer Gasse 5-11, 1120 Vienna, Austria

[3] Instituto de Medicina Molecular, Faculdade de Medicina, Universidade de Lisboa, Lisbon, Portugal

[4] present address: School of Biological Sciences, Faculty of Biology, Medicine and Health, University of Manchester, Michael Smith Building, Manchester, M13 9PT, UK

[‡] these authors contributed equally to this work

[*]correspondence should be addressed to: pawel.leznicki@manchester.ac.uk or ykulathu@dundee.ac.uk

Running title: Isoform-specific functions of USP35

Keywords: apoptosis/Deubiquitinase/endoplasmic reticulum/lipid droplets/ubiquitin signalling

SUMMARY STATEMENT

Here, we provide evidence that alternative isoforms can substantially contribute to expanding the functionality of deubiquitylating enzymes, hence allowing them to regulate the multitude of intracellular ubiquitylation events.

ABSTRACT

Protein ubiquitylation is a dynamic post-translational modification that can be reversed by deubiquitylating enzymes (DUBs). It is unclear how the small number of ~100 DUBs present in mammalian cells regulates the thousands of different ubiquitylation events. Here we analysed annotated transcripts of human DUBs and find ~300 ribosome-associated transcripts annotated as protein coding, which thus increase the total number of DUBs. Using USP35, a poorly studied DUB, as a case study we provide evidence that alternative isoforms contribute to the functional expansion of DUBs. We show the existence of two different USP35 isoforms that localise to different intracellular compartments and have distinct functions. Our results reveal that isoform 1 is an anti-apoptotic factor that inhibits staurosporine- and TNF-related apoptosis inducing ligand (TRAIL)-induced apoptosis. In contrast, USP35 isoform 2 is an integral membrane protein of the endoplasmic reticulum (ER) present also at lipid droplets. Manipulations of isoform 2 levels cause rapid ER stress likely through deregulation of lipid homeostasis and lead to cell death. Our work highlights how alternative isoforms provide functional expansion of DUBs and sets directions for future research.

INTRODUCTION

Covalent attachment of ubiquitin to target proteins, or ubiquitylation, regulates many critical intracellular processes such as signal transduction, protein turnover and trafficking. Ubiquitylation is achieved through a sequential action of E1 activating, E2 conjugating and E3 ligating enzymes, and can be reversed by deubiquitylating enzymes or deubiquitinases (DUBs) (Hershko and Ciechanover, 1998). Ubiquitylation usually occurs on lysine residues of a substrate protein. Importantly, one of the seven internal lysines or the N-terminal methionine of ubiquitin can serve as an attachment site for another ubiquitin, thus forming ubiquitin chains (polyubiquitin) whose linkage type determines the biological outcome of ubiquitylation (Yau and Rape, 2016)

The importance of protein ubiquitylation and deubiquitylation is underscored by the fact that deregulation of these processes has been linked to the pathogenesis of many human diseases such as cancer, and neurodegenerative and metabolic disorders (Heideker and Wertz, 2015; Popovic et al., 2014). In many cases, such detrimental outcomes stem from deregulation of key signalling pathways that are normally controlled by the ubiquitin system. For example, several DUBs have been implicated in the regulation of cell death either through controlling the stability of various pro- and anti-apoptotic factors or by regulating the formation of essential signalling complexes (Engel et al., 2016; Jeong et al., 2017; Lee et al., 2015; Mahul-Mellier et al., 2012; Mei et al., 2011; Schwickart et al., 2010; Weber et al., 2016).

Considering their profound roles in regulating cell fate and function we still know surprisingly little about the precise functions and substrates of many DUBs. Further, it is intriguing that a relatively small number of DUBs (~100 predicted to exist based on the human genome sequence) can regulate at least ~20,000 ubiquitin-modified sites that can be currently detected at steady-state conditions in mammalian cells (Clague et al., 2015; Kim et al., 2011; Udeshi et al., 2013). Whilst we are still far from understanding how this is achieved, several potential modes of expanding the functionality of DUBs have been proposed. These include alternative subcellular localization of DUBs, regulation by interacting proteins and post-translational modifications. An unappreciated mechanism is the expansion of DUB functionality via alternative splicing, which provides a way to increase the total number of DUBs that can perform distinct functions (Leznicki and Kulathu, 2017). However, with few exceptions, the presence and specific functions of alternative DUBs isoforms have been almost completely neglected.

In order to understand to what extent alternative isoforms contribute to the functional expansion of DUBs, we analysed a recent dataset of ribosome-associated transcripts from HEK293 cells (Floor and Doudna, 2016). Strikingly, we found that ~300 DUB transcripts annotated as protein coding associate with translating ribosomes in human cells. To address if DUB isoforms perform non-redundant functions, we chose a poorly studied DUB, USP35, as a case study. Here, we characterised USP35 using biochemical, structural and cell biological approaches. Intriguingly, we detect at least two different USP35 isoforms at the endogenous level that localise to distinct intracellular compartments. In contrast to isoform 1, which is a soluble protein, isoform 2 is a novel integral membrane protein that localises to the ER and lipid droplets. Remarkably, isoform 2 expression induces rapid ER stress most likely because of perturbed lipid homeostasis and leads to cell death. Isoform 1 has a distinct function and acts as an anti-apoptotic factor that inhibits TNF-related apoptosis inducing ligand (TRAIL)- and staurosporine-induced apoptosis. Our results highlight how products of a single DUB-encoding gene can have contrasting functions.

RESULTS

Alternative isoforms expand the number of DUBs

A number of transcripts associate with translating ribosomes in HEK293 cells, suggesting widespread production of alternative isoforms (Floor and Doudna, 2016). We analysed the results of this high-throughput study to get insights into the extent to which the functionality of DUBs could be expanded by the presence of DUB isoforms. Strikingly, we find that in HEK293 cells there are ~500 ribosome-associated DUB transcripts, of which ~300 are annotated as protein coding (Table S1). The number of protein coding DUB transcripts is likely an underestimation because mRNAs coding for some of the known DUBs such as OTUD6A and USP26 were not detected in the above-mentioned study (Floor and Doudna, 2016). Further, this estimation is based on HEK293 cells and given that isoforms are expressed in a tissue-specific manner (Buljan et al., 2012; Ellis et al., 2012; Yang et al., 2016), it is likely that the total number of DUB isoforms expressed is even greater. As many of the DUB transcripts lack annotated 5' or 3' ends, DUB-centred transcriptomics analyses will be required to define the precise boundaries of these isoforms. Importantly, isoform-specific peptides were detected for at least some of these putative isoforms confirming their existence in living cells (Wilhelm et al., 2014).

USP35 is an active, ubiquitin linkage type-promiscuous DUB

To explore how alternative isoforms expand DUB function, we here studied USP35, a member of the ubiquitin specific protease (USP) DUB family. Importantly, transcripts with annotated 5' and 3' ends coding for three different USP35 isoforms with intact catalytic domain were shown to associate with translating ribosomes (Floor and Doudna, 2016) (Fig 1A). The different USP35 isoforms are: full length ($USP35^{iso1}$), an isoform with an N-terminal truncation of 269 residues ($USP35^{iso2}$) and one lacking 432 residues at the N-terminus ($USP35^{iso3}$). Furthermore, high-throughput proteomic experiments identified unique acetylated N-terminal peptides specific for $USP35^{iso1}$ and $USP35^{iso2}$ (Wilhelm et al., 2014). USP35 is a poorly studied DUB suggested to play a role in mitophagy (Wang et al., 2015) and as a tumour suppressor (Liu et al., 2015). The latter finding is, however, at odds with reports showing that USP35 is amplified in a number of cancers, particularly breast and ovarian ((Chin et al., 2007) and www.cbioportal.org).

USP35 is characterised by the presence of a USP catalytic domain where cysteine 450 is the active site (Fig 1A). Similar to other USP DUBs that have insertions within their catalytic

domains, USP35 also has a long highly-charged ~150 residue loop insertion in its USP domain that spans residues 604-753 and is predicted to be unstructured (Ye et al., 2009). Based on the crystal structure of the N-terminal fragment of a closely related DUB, USP38 (Shen et al.) (PDB: 4RXX), it can be expected that USP35 also contains N-terminal HEAT repeats (Fig 1A), a motif known to mediate protein-protein interactions.

In order to investigate if USP35 is an active enzyme, we expressed and purified full-length human USP35^{iso1}. When tested for enzymatic activity against tetraubiquitins of defined linkage types, USP35 showed promiscuous activity and cleaved several linkages of which Lys11-, Lys33-, Lys48- and Lys63-linked polyubiquitin were cleaved most efficiently (Fig 1B). Such promiscuity is often found amongst members of the USP family of DUBs whose selectivity seems to be determined by a substrate rather than ubiquitin linkage type (Faesen et al., 2011).

To understand USP35 at the molecular level we attempted to crystallise catalytically inactive (C450S mutant) USP35$^{423-944}$, the fragment that spans the catalytic domain shared by all three isoforms, in complex with Lys48-linked diubiquitin. Since the full length catalytic domain was refractory to crystallization, we speculated that removing the disordered loop insertion within the catalytic domain would result in diffracting crystals. Indeed, we obtained crystals of the catalytic domain lacking this loop in complex with Lys48 diubiquitin that diffracted to 1.8Å (Fig 1C). The structure was solved by molecular replacement and refined to the statistics shown in Table S2. Importantly, bacterially purified catalytic domain of USP35 lacking the loop insertion shows similar activity and ubiquitin linkage type preference as the wild-type catalytic domain (Fig S1). Surprisingly, we could only detect a single ubiquitin in complex with USP35, which might result from the residual DUB activity of the C450S mutant used (data not shown). Hence, the structure represents USP35 in complex with the distal ubiquitin. The crystal structure of USP35 reveals a typical USP domain architecture that superposes well onto the structures of previously crystallised USP domains (Figs 1C and S2). Clearly defined subdomains referred to as thumb, palm and fingers can be observed in the structure (Fig 1C) (Yin et al., 2015). The bulk of ubiquitin until Arg72 is clasped between the thumb, palm and fingers subdomains by a strong network of hydrophobic, ionic and hydrogen bonds (Figs 1C and S3). The cation-π and aromatic-aromatic interactions between the fingers sub-domain and the ubiquitin molecule stabilise the complex (Fig S3). Clear electron density is visible for the catalytic triad of USP35, composed of Cys450, His862 and Asp895 (Figs 1C and S3E).

USP35 shows isoform-specific subcellular localisation

Since the three USP35 isoforms all contain an intact catalytic domain (Fig 1A), we wondered if the differences in the N-terminal region regulate their intracellular localisation. To address this possibility, we analysed the subcellular localisation of C-terminally GFP-tagged USP35 isoforms (Fig 2A). Strikingly, we observed that the intracellular distribution of the proteins analysed was isoform-specific. While USP35^{iso1} and USP35^{iso3} display a rather diffuse staining, USP35^{iso2} shows a reticular pattern, suggestive of endoplasmic reticulum (ER) localisation. Importantly, since the C-terminus of all isoforms analysed is identical, the differences observed in the staining pattern do not result from protein tagging. To determine which subcellular compartment USP35^{iso2} resides in, we performed co-localisation experiments that showed a clear overlap in the staining pattern of USP35^{iso2} and an endogenous ER marker, BAP31 (Ng et al., 1997) (Fig 2B), confirming that USP35^{iso2} localises to the ER.

Interestingly, in addition to the reticular ER staining, USP35^{iso2} forms doughnut-like structures that could potentially correspond to protein aggregates, intracellular vesicles or lipid droplets (Fig S4A). Interestingly, in a number of cells such doughnut-like staining of USP35^{iso2} was predominant, in particular when the detergent permeabilisation step during sample preparation was omitted. This suggests that these are lipid-based structures such as lipid droplets. Lipid droplets are intracellular organelles that originate from the ER and serve as primary storage sites of neutral lipids such as triglycerides and cholesterol esters (Welte, 2015). Given our finding that USP35^{iso2} localises to the ER and that the USP35^{iso2}-positive doughnut-like structures are likely detergent-sensitive, we investigated if they correspond to lipid droplets. Indeed, USP35^{iso2} co-localises with the dye LipidTox that stains lipid droplets (Fig 2C, top panel) and this co-localisation is even more pronounced in cells treated with oleic acid (Fig 2C, bottom panel), a condition that induces the formation and accumulation of lipid droplets (Eastman et al., 2009). These data indicate that in addition to ER localisation, USP35^{iso2} is also present at lipid droplets making it, to the best of our knowledge, the first lipid droplet-localising DUB.

USP35 isoform 2 is an integral ER membrane protein

ER localisation of proteins results either from their integration into the lipid bilayer or peripheral binding to other proteins or lipids. To understand how ER targeting of USP35^{iso2} is achieved, we analysed its amino acid sequence. Two potential, albeit relatively hydrophilic,

transmembrane domains (TMDs) predicted to span residues 317-337 and 797-815 (numbering based on iso1) were detected (Hessa et al., 2007). Helix 797-815 is located within the USP domain suggesting that it does not mediate ER localisation. The potential TMD comprising residues 317-337 is more hydrophobic and also predicted by an alternative TMD prediction algorithm, TMpred (http://www.ch.embnet.org/software/TMPRED_form.html). Prediction algorithms do not indicate an N-terminal signal peptide in USP35^{iso2} amino acid sequence and hence the predicted transmembrane domain could also act as an ER targeting signal (Shao and Hegde, 2011). Indeed, a short USP35 fragment, USP35$^{245-432}$, still co-localises with BAP31 indicating that the ER targeting motif is located within this sequence in agreement with the prediction for a putative TMD (Fig 2D).

To experimentally address if USP35^{iso2} is an integral membrane protein, we performed protease protection experiments using U2OS FlpIn cells expressing USP35 isoforms fused to GFP either at the N- or C-terminus. Cells were treated with digitonin that selectively permeabilises the cholesterol-rich plasma membrane while maintaining the integrity of the cholesterol-poor ER membrane. This in turn allows for trypsin-mediated digestion of cytosolically exposed protein regions whilst leaving the ER luminal proteins intact due to the inability of the protease to access the ER lumen. When calnexin (CNX), a model ER membrane protein, was tested, addition of trypsin resulted in the cleavage of its cytosolic portion as assessed by the increase in its electrophoretic mobility (Fig 3A). When the same analysis was carried out for GFP-tagged USP35 isoforms, an anti-GFP antibody-reactive, protease-protected species was apparent only when N-terminally tagged USP35^{iso2} was expressed (Fig 3A, lane 6, red dot). Importantly, the ~37 kDa size of this fragment corresponds to the size of GFP-tagged USP35$^{270-360}$ that would be generated by trypsin cleavage if residues 317-337 constitute the TMD (~27 kDa GFP tag and ~10 kDa mass of amino acids 270-360). No trypsin-resistant fragments were observed when iso1 or C-terminally tagged iso2 were used indicating complete proteolysis of their GFP tag (Fig 3A). The results obtained using the protease protection assay clearly show that iso2 is an integral membrane protein with its N-terminus in the ER lumen.

To further confirm our results, we used an assay that monitors N-glycosylation of ER-destined proteins (Borgese et al., 2001; Leznicki et al., 2010). Importantly, N-glycosylation takes place in the ER lumen and hence can be used as an independent read-out for the luminal localisation of a protein or its portion. Hence, we fused USP35^{iso2} to a short peptide derived from bovine rhodopsin (OPG) that contains two N-glycosylation sites (Borgese et al., 2001)

and transiently expressed it in U2OS FlpIn cells. Consistent with the results of the protease protection assay, N-glycosylation of iso2 was only observed when the OPG tag was placed at its N-terminus as assessed by the change in the electrophoretic mobility following endoglycosidase H (EndoH) treatment (Fig 3B, lanes 1 and 2, OPG-iso2 panel). Consistent with amino acids 317-337 acting as the TMD, a short fragment of USP35, $USP35^{270-432}$, is efficiently N-glycosylated when fused to the OPG tag (Fig 3C). Interestingly, in this case the orientation of the TMD is random as evidenced by the modification of both the N- and C-terminally tagged $USP35^{270-432}$. This is most likely caused by the small size of the fragment used and suggests that the C-terminal portion, i.e. the catalytic domain may play a role in dictating the topology.

The ER targeting motif of $USP35^{iso2}$ is also present in iso1 yet we found no evidence of its ER membrane integration. We speculated that this might be caused by the presence of the intact N-terminal HEAT repeats in iso1 that are truncated in iso2 (Fig 1A). To investigate if the length of the HEAT repeats affects ER integration of USP35 we generated truncated variants of USP35 bearing an N-terminal OPG tag and assessed their integration into the ER membrane using N-glycosylation as a read-out. Indeed, we observed that whilst $USP35^{iso2}$ and $USP35^{180-1018}$ are efficiently inserted into the ER lipid bilayer, increasing the length of the N-terminal HEAT repeats abolishes USP35 integration into the ER membrane (Fig 3D). This argues for the role of HEAT repeats in limiting ER integration of $USP35^{iso1}$. Taken together, we conclude that $USP35^{iso1}$ is a soluble, predominantly cytosolic protein whilst $USP35^{iso2}$ is an integral membrane protein of the ER with its N-terminus in the ER lumen and C-terminus together with the USP domain facing the cytosol (Fig 3E). Importantly, the sequence of the proposed transmembrane region is highly conserved in vertebrates (Fig 3E).

It was previously reported (Buljan et al., 2012; Ellis et al., 2012; Yang et al., 2016) that the relative abundance of protein isoforms differs depending on the cell type and tissue analysed, and we wondered if the same applied to USP35. We therefore raised antibodies that recognise the N-terminal (AbN), middle (Ab2) or C-terminal (AbC) portions of USP35 (Fig 1A) and used AbC (that should recognise both isoforms 1 and 2) to screen a panel of different cell lines (Fig S4B). In all cell lines tested, we could clearly detect a protein species that we identify as $USP35^{iso1}$ based on its electrophoretic properties (Fig S4B) and sensitivity to siRNA-mediated depletion (Fig S4C)

Interestingly, in two cell lines, pancreatic cancer cell line HPAF-II and lung cancer cell line NCI-H1435, we could also detect an additional USP35 protein species that could correspond to $USP35^{iso2}$ based on its electrophoretic mobility (Fig S4B). To verify if this protein is

indeed USP35^{iso2}, we tested its localisation by performing subcellular fractionation of HPAF-II cells (Fig 3F). To aid in the assignment of USP35 isoform bands we used lysates of HPAF-II cells transfected with plasmids encoding untagged USP35^{iso1} and USP35^{iso2}. Our results showed that USP35^{iso1} is predominantly cytosolic (Fig 3F). Strikingly, we could also detect a protein species with electrophoretic migration identical to that of ectopically expressed untagged USP35^{iso2} (Fig 3F, "USP35 long exp." panel). Importantly, as expected for an integral membrane protein, this anti-USP35 antibody-reactive species was recovered exclusively in the membrane fraction (Fig 3F, "USP35 long exp." panel). To further confirm the existence of USP35^{iso2} at the endogenous level we immunoprecipitated USP35 from HPAF-II cells (Fig 3G). This approach allowed us to recover two USP35 species that migrate with similar electrophoretic mobility as isoforms 1 and 2 (Fig 3G). Based on their electrophoretic properties, reactivity with three distinct anti-USP35 antibodies and results of the subcellular fractionation experiments we infer that these two species correspond to USP35 isoforms 1 and 2.

USP35 isoform 2 induces ER stress and apoptosis

We next wanted to understand if USP35 isoforms 1 and 2 perform isoform-specific functions. Intriguingly, when investigating the intracellular localisation of USP35 we noticed that cells expressing USP35^{iso2} in many cases showed altered BAP31 staining that resembled aggregate-like structures (Fig 4A). To test if this was due to a general aggregation of the ER membrane, we monitored the staining for signal peptide peptidase (SPP), another integral ER membrane protein. Localisation of SPP was unchanged suggesting that the punctate staining of BAP31 was specific (Fig 4A). Formation of BAP31 punctae reflects BAP31 cleavage by caspase-8 during apoptosis (Maatta et al., 2000), and expression of USP35^{iso2} results in BAP31 cleavage as indicated by its increased electrophoretic mobility (Fig 4B). Further, BAP31 cleavage is accompanied by activation of caspase-8 and caspase-3 (Fig 4B). Expression of USP35^{iso2} also causes ER stress that is evident by increased levels of the ER luminal chaperone, BiP (Fig 4B). Importantly, a control ER-membrane localising construct, GFP fused to the ER targeting sequence of cytochrome b5 (GFP-b5) (Bulbarelli et al., 2002), does not induce the same phenotype indicating the specificity of USP35^{iso2} action (Fig 4B, lanes 1 and 2). Consistent with the observed apoptotic events, overexpression of USP35^{iso2} blocks cell proliferation (Fig 4C).

ER stress initiates signalling events that result in improved folding capacity of the ER, for example, by upregulating the expression of luminal chaperones and blocking general protein

translation (Tabas and Ron, 2011). Unresolved ER stress, however, triggers apoptosis through the action of protein kinase PERK and its target CHOP, a transcription factor. CHOP activates transcription of several pro-apoptotic genes including death receptor 5 (DR5), a cell surface receptor for ligands such as TNF related apoptosis inducing ligand (TRAIL) that stimulate the extrinsic apoptotic pathway (Lu et al., 2014). Importantly, ER stress induced, CHOP-mediated upregulation of DR5 has been proposed to activate caspase-8 leading to apoptosis (Lu et al., 2014). However, the precise function of caspase-8 in ER stress induced cell death is debated with some studies arguing against such a role for caspase-8 (Glab et al., 2017). In order to establish if USP35^{iso2} expression also upregulates markers of ER stress induced apoptosis we monitored protein levels of CHOP and DR5 following USP35^{iso2} expression (Fig 4D). Inducing USP35^{iso2} expression for 24h resulted in significantly elevated levels of CHOP and DR5 and this effect was blocked by simultaneous treatment with GSK2606414, an inhibitor of PERK (Axten et al., 2012) (Fig 4D). Importantly, in addition to U2OS FlpIn cells used so far, we observe the same role of USP35^{iso2} in inducing ER stress and cell death in HeLa FlpIn cells (Fig. 4E), indicating that USP35^{iso2} function is conserved. Interestingly, while caspase-3 is clearly activated in HeLa FlpIn cells expressing USP35^{iso2}, no processing of caspase-8 was detected, which is at odds with our findings using U2OS FlpIn cells. This is, however, consistent with conflicting reports about the role of caspase-8 in inducing cell death during conditions of ER stress (Glab et al., 2017; Lu et al., 2014). We then sought to understand the kinetics of USP35^{iso2}-mediated ER stress. To this end, expression of C-terminally tagged USP35^{iso2} was induced and ER stress monitored over time. Strikingly, BiP expression was already elevated after 10h induction of USP35^{iso2}, which is only 4h after the protein is detectable by Western blotting (Fig 4F). To further assess the specificity of USP35^{iso2}-induced ER stress and apoptosis we created U2OS FlpIn cell line expressing GFP-tagged USP19, the only reported integral membrane DUB of the ER. Importantly, expression of USP19 at levels comparable to USP35^{iso2} did not induce apoptosis or detectable ER stress (Fig 4G). Collectively, our results suggest that ectopic USP35^{iso2} expression causes specific and rapid ER stress and apoptosis.

USP35^{iso2}-mediated ER stress results from misregulated lipid homeostasis and is uncoupled from apoptosis induction

Given the lipid droplet localisation of USP35^{iso2} and links between the ER and lipid metabolism we speculated that USP35^{iso2} induces ER stress and cell death by interfering with some aspects of lipid homeostasis. Because lipid droplets are the primary storage sites for

cholesterol esters we investigated if USP35^{iso2} induced ER stress and apoptosis might result from aberrations of cholesterol metabolism. Hence, we followed the effect of USP35^{iso2} expression on ER stress in the presence of mevastatin and lovastatin, inhibitors of 3-hydroxy-3-methyl-CoA reductase (HMGCR), a rate-limiting enzyme of cholesterol biosynthesis. Strikingly, we observed that inhibiting HMGCR significantly reduces USP35^{iso2}-induced ER stress as measured by BiP upregulation (Figs 5A and B). Importantly, inhibiting cholesterol biosynthesis had no effect on ER stress initiated by disrupting ER calcium homeostasis (Fig 5A). Taken together, these results imply that inhibiting cholesterol synthesis specifically interferes with early steps of ER stress induced by USP35^{iso2} rather than downstream events general to ER stress response. Surprisingly, inhibiting cholesterol synthesis prevents USP35^{iso2}-induced ER stress but does not impede caspase-8 and caspase-3 activation, suggesting that ER stress and apoptosis induced by USP35^{iso2} could be unrelated events. To exclude the possibility that the inhibitory effect of statins was an indirect consequence of depleting cholesterol, we expressed USP35^{iso2} in U2OS FlpIn cells grown in media containing lipoprotein deficient serum (LPDS) and assessed ER stress by monitoring BiP levels (Fig S5A). We found that while LPDS treatment efficiently lowered cellular cholesterol levels as measured by upregulation of low density lipoprotein receptor (LDLR), it did not block USP35^{iso2}-induced ER stress. Hence, we conclude that cholesterol *per se* is not required for the induction of ER stress by USP35^{iso2} but rather USP35^{iso2} expression interferes with lipid homeostasis possibly by affecting the cholesterol and/or isoprenoids biosynthetic route.

To further explore the links between USP35^{iso2}-mediated ER stress and apoptosis we expressed various USP35^{iso2} truncations and assessed their capacity to induce ER stress and apoptosis. We observed that USP35^{iso2} lacking the insertion loop within the catalytic domain (Fig 1A) was more efficient at inducing apoptosis than the wild-type protein despite lower capacity to induce ER stress (Fig 5C). Importantly, expression of USP35^{iso2} lacking the predicted ER luminal residues (amino acids 270-316) no longer triggered ER stress and apoptosis (Fig 5C). Whilst it is unclear why deletion of the insertion loop from USP35^{iso2} increases its capacity to induce apoptosis yet lowers the extent of ER stress that it induces, this result again shows that apoptosis is not a simple consequence of ER stress caused by USP35^{iso2} expression. Hence, these observations suggest that the ER stress and apoptosis induced by USP35^{iso2} are two distinct phenomena.

To further investigate this possibility, we tested the effect of the PERK inhibitor GSK2606414 on cells expressing USP35^{iso2} (Fig S5B). Again, we found that GSK2606414

almost completely blocked ER stress induced by USP35^{iso2} (Fig S5B, compare lanes 1 and 4, see also Fig 4D). Despite the loss of ER stress, the cells still exhibited apoptosis albeit to a lesser extent than in control cells. Interestingly, a recent study showed that GSK2606414 is also a potent inhibitor of RIPK1-mediated apoptosis and necroptosis (Rojas-Rivera et al., 2017). Hence, an "off-target" effect of GSK2606414 on apoptosis independent of ER stress is likely and could explain the apparent discrepancy between the effect of GSK2606414 and statins on USP35^{iso2}-induced apoptosis. Nonetheless, the fact that GSK2606414 failed to completely block USP35^{iso2}-induced apoptosis lead us to conclude that ER stress and apoptosis induced by USP35^{iso2} are unrelated events.

To investigate if the ability of USP35^{iso2} to induce ER stress and apoptosis is linked to ER membrane/lipid droplet localisation we performed subcellular fractionation and pull-down assays from cells expressing GFP-tagged wild-type USP35 and its variants lacking either the insertion loop or luminal residues. Indeed, we observed that variants that induce ER stress and apoptosis efficiently co-fractionate with cellular membranes (Fig 5D) and interact with lipid droplet-associated protein, PLIN2 (Fig 5E). Such shared requirements for membrane localisation and lipid droplet association are in agreement with previous reports showing that localisation to these two organelles can be mediated by the same hydrophobic domain (Bersuker et al., 2018; Zehmer et al., 2008). USP35^{iso2} lacking residues 270-316 only weakly associated with membranes (Fig 5D) suggesting that these residues contribute to the ER membrane localisation of USP35^{iso2}. These findings demonstrate the importance of membrane/lipid droplet localisation of USP35^{iso2} for the induction of ER stress and apoptosis. To further verify this conclusion, we fused GFP-tagged USP35 fragments to the first 61 residues of SPP that encompass its first transmembrane domain with a topology that ensures cytosolic localisation of USP35 catalytic domain. Strikingly, we observed that such enforced ER membrane localisation of soluble fragments of USP35 spanning residues 338-1018 and 433-1018 (which corresponds to isoform 3) was sufficient to induce both ER stress and apoptosis (Fig 5F). However, targeting GFP alone to the ER using the same tag does not produce the effects observed with USP35. Hence, ER membrane anchoring of USP35 catalytic domain is sufficient to induce ER stress and apoptosis.

USP35^{iso1} is an anti-apoptotic protein

In order to compare the functions of isoforms 1 and 2 of USP35, we tested the effect of their overexpression on the induction of ER stress and apoptosis. Consistent with our previous data (Fig 4) increased levels of USP35^{iso2} led to the induction of apoptosis (Fig 6A). In contrast,

USP35^{iso1} did not induce the same phenotype (Fig 6A) suggesting distinct functions for these two isoforms, in line with their distinct intracellular localisation.

The *D. melanogaster* orthologue of USP35 and USP38, DUBAI, has previously been shown to be an anti-apoptotic protein (Yang et al., 2014). To test if USP35^{iso1} has the same function in mammalian cells, we monitored apoptosis in HEK293 cells overexpressing USP35^{iso1} following the apoptotic stimulus, TRAIL, by monitoring cleavage of caspase-8, the main initiator caspase of the extrinsic apoptotic pathway. Compared to control cells, cells expressing increased levels of USP35^{iso1} exhibit delayed processing of caspase-8 during TRAIL-induced apoptosis (Fig 6B). Importantly, this anti-apoptotic effect required the catalytic activity of USP35^{iso1} (Fig 6B, lanes 9-16 and 17-24). Since overexpression has an anti-apoptotic effect, we posited that depletion of USP35 would result in an opposite effect, i.e. sensitise cells to apoptotic stimuli. To address this possibility, we deleted USP35 using CRISPR/Cas9-mediated gene editing. Indeed, we observed that USP35 knock-out cells are substantially more sensitive to TRAIL-induced apoptosis as assessed by activation of caspase-8 (Fig 6C). Consistent with such increased processing of caspase-8 upon USP35 depletion, USP35 knock-out cells are significantly more sensitive to TRAIL treatment (Fig 6D). Further, we also observed increased sensitivity of USP35 knock-out clones to staurosporine-induced apoptosis as assessed by activation of caspase-3 (Fig 6E). Our results reveal that in contrast to USP35^{iso2}, isoform 1 has an anti-apoptotic function.

A common feature of many anti-apoptotic proteins such as inhibitors of apoptosis proteins (IAPs) is their proteolytic processing during apoptosis (Hao et al., 2004; Hornle et al., 2011), which leads to their inactivation and allows for progression of cell death. We therefore wanted to investigate if iso1 of USP35 is also a subject of such processing. To test this possibility, we induced apoptosis with staurosporine in HeLa cells that express USP35^{iso1} at relatively high levels (Fig S4B). Strikingly, endogenous USP35 was efficiently cleaved during staurosporine-induced cell death (Figs S6A, B). The cleaved fragments could be recovered by immunoprecipitation using antibodies raised against the N- or C-terminal parts of USP35 with the N-terminal fragment being ~85 kDa and the C-terminal one ~30 kDa (Fig S6B). This USP35 proteolysis could be blocked by zVAD-fmk, a pan-caspase inhibitor, suggesting that the processing is mediated by caspase(s) (Figs S6A, B). Indeed, *in vitro* caspase cleavage assay indicates that proteolysis of USP35 is mediated by the executioner caspases, caspases -3 and/or -6 (Fig S6C). Mass spectrometric analyses identified D743 as the cleavage site, a finding consistent with the size of USP35 fragments observed in HeLa cells undergoing apoptosis (Figs S6A, B). Indeed, mutation of the cleavage site D743 to

alanine completely blocked USP35 proteolysis during staurosporine-induced apoptosis (Fig 6F). In summary, our findings reveal that USP35^{iso1} is an anti-apoptotic protein and suggest a model where proteolytic cleavage by caspases at D743 within the USP35 catalytic domain inactivates the DUB and thereby its anti-apoptotic function.

USP35 isoform-specific interactome

The fact that USP35^{iso1} is anti-apoptotic and USP35^{iso2} pro-apoptotic suggests that these two proteins might exert their effects by differentially regulating a common interacting partner(s). To investigate this possibility, we identified the binding partners of both USP35 isoforms using HEK293 FlpIn cell lines expressing USP35 isoforms C-terminally tagged with BirA^{R118G}. This allows for the use of the BioID methodology capable of identifying interactions transient in nature or occurring in organelles resistant to conventional immunoprecipitation techniques (Roux et al., 2012). In agreement with distinct subcellular localisation of USP35^{iso1} and USP35^{iso2} we found that the GO terms associated with their interacting partners are differently enriched (Fig 7A). Hence, USP35^{iso2} preferentially interacts with proteins linked to intracellular membranes, in particular the ER. In contrast, USP35^{iso1} interacts predominantly with cytosolic and centrosomal proteins. Importantly, USP35^{iso2} interacted with a number of enzymes linked to lipid metabolism (HMGCR, CYP51A1, AGPAT4) and protein quality control (TRIM13, BAG6, UBE2J1, UBR3) (Fig 7B and Table S3). Only ~15% of the total binding partners were shared by the two USP35 isoforms confirming their distinct functions. Interestingly, among the common interacting proteins was BIRC6, a known IAP (Bartke et al., 2004; Hao et al., 2004), which could potentially be targeted by both USP35 isoforms. To test if USP35 isoforms act on the same pathway regulating apoptosis we tested if USP35^{iso1} can inhibit USP35^{iso2}-induced apoptosis. Cells expressing USP35^{iso2} in an inducible manner were transfected with USP35^{iso1} at the time of USP35^{iso2} induction, and upregulation of BiP and caspase-3 cleavage were monitored. This revealed that USP35^{iso1} cannot block USP35^{iso2}-induced apoptosis (Fig S6D) suggesting that the two isoforms regulate different aspects of apoptosis.

DISCUSSION

In the current study we show that mammalian cells express at least two USP35 isoforms that localise to distinct subcellular compartments and have distinct functions. Isoform 1 is an anti-apoptotic protein that regulates progression of TRAIL- and staurosporine-induced apoptosis. At the same time, isoform 2 is a novel integral membrane protein that localises to the ER and lipid droplets, its overexpression perturbs lipid homeostasis and causes ER stress and apoptosis.

Interestingly, until now USP19 was the only known DUB that is an integral ER membrane protein (Hassink et al., 2009). USP35^{iso2} that we identified in this study becomes the second integral ER membrane DUB. Intriguingly, just like we observe for USP35 also USP19 exists in at least two forms, cytosolic and ER membrane-localised, that have non-redundant functions (Hassink et al., 2009; Lee et al., 2016). Moreover, USP35^{iso2} is, to the best of our knowledge, the first lipid droplet associated DUB. Lipid droplets perform important functions that extend beyond lipid storage and mobilisation. These include protein sequestration and degradation evidenced by the presence of ubiquitin-conjugating machinery at lipid droplets (Klemm et al., 2011; Spandl et al., 2011; Welte, 2015). Moreover, lipid droplet dynamics is also regulated by protein ubiquitylation (Eastman et al., 2009) and hence our discovery of a lipid droplet associated DUB opens new avenues of research.

Surprisingly, USP35^{iso1} and USP35^{iso2} both contain the same ER membrane targeting motif yet we observe that only iso2 inserts into the ER lipid bilayer. Based on our data we postulate that the N-terminal HEAT repeats present in iso1 but truncated in iso2 mediate either co-translational folding or recruitment of interacting factors that prevent ER delivery of iso1. Indeed, the inhibitory effect of co-translational folding on protein translocation into the ER is well documented (Conti et al., 2014; Denzer et al., 1995). Removal of the N-terminal 269 residues as seen in USP35^{iso2} would disrupt the HEAT repeat motif composed of consecutive alpha helices that form extensive contacts with each other. This in turn would allow for efficient ER targeting. Interestingly, addition of an N-terminal GFP tag to USP35^{iso2} does not block its integration into the ER membrane indicating that specific interactions of the N-terminal portion of iso1 are required to prevent its ER delivery.

Strikingly, we observe that ectopic expression of USP35^{iso2} induces rapid ER stress and apoptosis in different cell lines. We show that ER stress initiated by USP35^{iso2} can be attenuated by inhibition of the rate-limiting enzyme of cholesterol biosynthesis, HMGCR, suggesting that it most likely results from perturbed lipid homeostasis. Imbalance in lipid metabolism can alter the composition of the ER membrane causing “lipid bilayer stress” (Han

et al., 2010; Pineau et al., 2009; Promlek et al., 2011; Thibault et al., 2012) and our data suggest that USP35^{iso2} might contribute to this effect. Importantly, we also show that anchoring soluble fragments of USP35 to the ER membrane is sufficient to induce both ER stress and apoptosis. The precise mechanistic details behind USP35^{iso2}-mediated ER stress remain to be uncovered. However, growing incidence of metabolic disorders linked to cholesterol metabolism and ER stress such as atherosclerosis warrants future studies on USP35^{iso2}.

Interestingly, our data indicate that the two phenotypes, ER stress and apoptosis, induced by USP35^{iso2} are unrelated. Intriguingly, our transcriptomics analyses indicate that total mRNAs coding for USP35^{iso2} is more abundant than mRNA encoding iso1 in cell lines and human tissues. However, at the protein level, USP35^{iso1} is the predominant USP35 species (Figs S4B, S7A, B). It is tempting to speculate that protein levels of USP35^{iso2} are kept low in order to avoid ER stress and apoptosis. However, the abundance of USP35^{iso2} mRNA would allow for its rapid translation in response to a yet unknown stimulus. Because USP35^{iso2} levels do not appear to increase following proteasome inhibition with MG132 (Fig S4C), we think that USP35^{iso2} protein levels are controlled at the translation step rather than through regulated protein degradation. A similar relief of miRNA-inhibited protein translation during conditions of stress has been reported for the cationic amino acid transporter 1 (CAT-1) (Bhattacharyya et al., 2006), establishing a paradigm for such a mechanism. Interestingly, USP35 is amplified in a number of cancers ((Chin et al., 2007) and Table S4 for USP35 copy number in selected cancer cell lines) and our analysis indicates that also in most primary tumours, USP35^{iso2} is preferentially transcribed (Fig S7C). Identification of stimuli that induce USP35^{iso2} production at the protein level will be of key importance for deciphering its molecular function.

We show that in contrast to USP35^{iso2}, USP35^{iso1} is a novel anti-apoptotic protein. This is evident using both overexpression and knock-out systems and assaying apoptosis in response to TRAIL and staurosporine treatments. Hence, USP35 is a hitherto unstudied DUB that regulates programmed cell death. This is consistent with the role of DUBAI, the *D. melanogaster* orthologue of mammalian USP35 and a related DUB, USP38 (Yang et al., 2014). DUBAI protects cells from apoptosis by stabilising DIAP1, a major IAP in fly. Although details of apoptotic pathways differ to some extent between fly and mammals, we provide evidence that the function of DUBAI as an anti-apoptotic factor is evolutionary conserved, and in mammals carried out by USP35^{iso1}. Consistent with anti-apoptotic roles, USP35 is amplified in a number of cancers, in which preferential translation of USP35^{iso1}

would block apoptosis and ensure cancer cell survival. Interestingly, we observe that both USP35^{iso1} and USP35^{iso2} interact with a mammalian IAP, Birc6 (Bartke et al., 2004; Hao et al., 2004). It remains to be tested if this interaction plays a role in the observed anti- and pro-apoptotic effects of USP35^{iso1} and USP35^{iso2}, respectively.

Consistent with distinct subcellular localisation our proteomic analysis indicates that USP35 isoforms interact mostly with distinct sets of proteins. While USP35^{iso2} interacts predominantly with membrane-associated proteins, USP35^{iso1} binds preferentially cytoplasmic and centrosomal proteins. The latter finding suggests that USP35^{iso1} could participate, for example, in regulating cell division. Indeed, during the preparation of this manuscript it was reported that USP35 stabilises Aurora B, a key kinase regulating mitotic progression, and USP35 depletion results in cytokinesis defects (Park et al., 2018). At the moment it is unclear if and how the anti-apoptotic effect of USP35^{iso1} is related to its function in stabilising Aurora B. Intriguingly, Birc6 has also been implicated in cytokinesis (Pohl and Jentsch, 2008) and future studies will establish if the cytokinesis defects observed following USP35 depletion result solely from its effect on Aurora B or if USP35-Birc6 interaction also plays a role.

Current proteomic datasets indicate that at least ~20,000 sites are modified with ubiquitin at steady state conditions in human cells (Kim et al., 2011; Udeshi et al., 2013), and it is therefore a massive endeavour for the relatively small number of ~100 DUBs to regulate them. Our results provide an important paradigm that alternative protein isoforms are of key importance for the expansion of DUB functionality and stress the need to study DUB isoforms. However, dissecting isoform-specific cellular functions is challenging and will require development of novel approaches such as the ability to selectively deplete only one isoform. We anticipate that studying functions of different isoforms in different experimental settings will reveal not only new DUB biology but also the true extent to which DUBs regulate cell physiology.

MATERIALS AND METHODS

Materials

Anti-USP35 antibodies were made to order by immunising sheep with glutathione S transferase (GST)-tagged recombinant fragments corresponding to USP35 residues: 1-437 (AbN), 604-753 (Ab2) and 925-1018 (AbC). Anti-GST-reactive antibodies were subsequently depleted by passing the sera through a resin containing immobilised recombinant GST. These antibodies were used at 0.1 μg/ml for Western blotting and 2-3 μg per 1 mg of cell lysate for immunoprecipitation. The following commercial antibodies were used for Western blotting: rabbit anti-GFP (1:7500, Abcam, ab6556), rabbit anti-calnexin (1:1000, Cell Signalling Technology, 2679), mouse anti-α-tubulin (1:10 000, Cell Signalling Technology, 3873), mouse anti-caspase-8 (1:1000, Cell Signalling Technology, 9746), rabbit anti-caspase-8 (1:1000, Tocris, AF1650-SP), rabbit anti-cleaved caspase-3 (1:1000, Cell Signalling Technology, 9661), rabbit anti-BiP (1:1000, Cell Signalling Technology, 3177), rabbit anti-BAP31 (1:1000, ProteinTech, 11200-1-AP), mouse anti-CHOP (1:1000, Cell Signalling Technology, 2895P), rabbit anti-DR5 (1:1000, Cell Signalling Technology, 8074), mouse anti-GAPDH (1:10000, Abcam, ab8245). Mouse monoclonal anti-OPG tag antibodies (used at 1:1000 dilution) were a kind gift of Prof. Stephen High (University of Manchester) and were as published before (Adamus et al., 1991). Antibodies used for immunofluorescence microscopy were as follows: chicken anti-GFP (1:2000, Abcam, ab13970), rat anti-BAP31 (1:2000, Abcam, ab15044), rabbit anti-SPP (1:200, Bethyl Laboratories, A304-404A).

Oleic acid-albumin complexes were purchased from Sigma Aldrich (O3008), LipidTox Deep Red Neutral Lipid Stain from Thermo Fisher Scientific (H34477), Endoglycosidase H from New England Biolabs (P0703), MTS assay kit from Promega (G3582), human recombinant TRAIL from Peprotech (310-04), zVAD-fmk from Enzo Life Sciences (ALX-260-020-M001). GSK2606414 (5107), mevastatin (1526) and lovastatin (1530) were obtained from Tocris.

Cell culture methods

HeLa FlpIn T. rex and HEK293 FlpIn T. rex were obtained from ThermoFisher Scientific, HPAF-II cells from ATCC whilst U2OS FlpIn T. rex cells were as previously reported (Bago et al., 2014). All cell lines were regularly tested for contaminations. U2OS FlpIn T. rex, HeLa FlpIn T. rex and HEK293 FlpIn T. rex cells were grown in DMEM supplemented with 10%

(v/v) FBS, 2 mM L-glutamine, 100 U/ml penicillin, 100 µg/ml streptomycin. HPAF-II cells were grown in EMEM supplemented with 10% (v/v) FBS, 2 mM L-glutamine, 100 U/ml penicillin, 100 µg/ml streptomycin, 1 mM sodium pyruvate and non-essential amino acids. Stable cell lines were generated by co-transfecting cells with pOG44 and plasmids encoding indicated proteins followed by selection in complete media containing 100 µg/ml hygromycin and 7.4 µg/ml blasticidin. Protein expression in stable cell lines was induced by addition of tetracycline to a final concentration of 200 ng/ml (U2OS FlpIn T.rex cells) or 1 µg/ml (HEK293 FlpIn T.rex cells).

DNA transfection was carried out using GeneJuice (Merck Millipore) according to manufacturer's instruction. For cell treatment with oleic acid the media was replaced with DMEM supplemented with 0.3 mM oleic acid-BSA complexes (Sigma Aldrich), and cells were incubated for additional 24h. Cells were also treated with 20 µM MG132 for 7h, 50 ng/ml recombinant human TRAIL (Peprotech) and 1 µM staurosporine for the times indicated.

Mevastatin and lovastatin were used at 10 µM and added simultaneously with tetracycline-mediated induction of USP35^{iso2}. Cells were then incubated for 48h. Alternatively, parental cells were treated with statins for 2h, 100 nM thapsigargin was added and cells were further incubated for 18h.

USP35 knock-out clones were generated by targeting exon 7 shared by all isoforms tested (sense gRNA gCATCCTTCAGGCCTTATTCA, antisense gRNA gTGACATAGCATGTGTTGCCC). Cells transfected with plasmids encoding these gRNAs and Cas9 were sorted into 96-well plates and clones derived from single cells screened by Western blotting. Candidate knock-out clones used for subsequent experiments were verified by sequencing of the targeted locus.

Fluorescence microscopy

Cells were grown on coverslips in 6-well plates and processed as described in figure legends. After washing with PBS, cells were fixed with 4% paraformaldehyde (PFA) for 15 min at RT. PFA was quenched by three consecutive washes with PBS supplemented with 100 mM glycine pH 8.0 (5 min each) and cells permeabilised with 0.1% (w/v) TX-100 for 5 min, RT. TX-100 was washed off with PBS and samples blocked with 1% (w/v) BSA in PBS for 15 min, RT. Coverslips were stained with chicken anti-GFP (Abcam, 1:2000), rat anti-BAP31 (Abcam, 1:2000) and rabbit anti-SPP (Bethyl Laboratories, 1:200) antibodies for 1h, RT.

Incubation with secondary antibodies (AlexaFluor conjugates, 1:750) was carried out for 30 min and coverslips were mounted using ProLong Gold reagent.

For lipid droplet staining cells were fixed, PFA quenched as described above and coverslips stained with LipidTox Deep Red (Life Technologies, 1:400) for 45 min, RT.

Samples were imaged using DeltaVision fluorescence microscopes and images processes by deconvolution with Softworx software.

Protein purification and in vitro assays

The pFastBac expression vectors encoding full-length human GST-USP35 and GST-USP35 C450A were used to generate recombinant baculoviruses using the Bac-to-Bac system (Invitrogen) following the manufacturer's protocol. These baculoviruses were used to infect *Spodoptera frugiperda* 21 cells (1.5×10^6/ml) at a multiplicity of infection of 5 and the infected cells were harvested 48 hours post-infection. GST-USP35 and GST-USP35 C450A were purified on GSH-Sepharose and dialysed into 50 mM Tris-HCl pH 7.5, 0.1 mM EGTA, 150 mM NaCl, 270 mM sucrose, 0.03% Brij-35, 0.1% 2-mercaptoethanol, 1 mM benzamidine, 0.1 mM phenylmethylsulfonyl fluoride (PMSF).

In vitro caspase cleavage assay was performed with Caspases Set III, human, recombinant Kit (#PK-RP577-K232, PromoKine), as per manufacturers instruction. In brief, 2 U of active recombinant human caspases were incubated with 4 μg purified human $USP35^{C450A}$ in buffer C (50 mM Hepes, pH 7.2, 50 mM NaCl, 0.1% (w/v) Chaps (3-[(3-cholamidopropyl)-dimethylammonio)-1-propanesulfonate), 10 mM EDTA, 5% (w/v) Glycerol, 10 mM DTT) for 2 h at 37°C.

DUB assays were carried out with 375 nM of USP35 and 733 nM of tetraUb of different linkage types (M1, K6, K11, K29, K33, K48 and K63) in 10 μl volume, in buffer D (50 mM Tris-HCl pH 7.5, 50 mM NaCl, 10 mM DTT) at 37°C for the times indicated. Reactions were quenched by adding LDS sample loading buffer.

Protein crystallisation

A construct of USP35 encoding amino acids S423-P944 with a deletion of E604-C753 (codon optimized for expression in Sf9cells) was generated by gene synthesis (GeneArt, Thermo Fisher Scientific) and expressed from a pDEST20 vector (Thermo Fisher Scientific) in Trichoplusia ni insect cells (High Five, Thermo Fischer Scientific) in Insect-XPRESS medium (Lonza) as an N-terminal GST-fusion protein (cleavable by tobacco etch protease,

TEV). Cells were collected after 48 hours and homogenized by a Dounce tissue grinder in PBS, 10% glycerol, 5 mM DTT, pH 7.3, in the presence of protease inhibitors (Complete, Roche Applied Science). After centrifugation at 11,000 x g (Beckman JA-10) the supernatant was batch-bound to a glutathione resin (Glutathione Sepharose, GE Healthcare). The resin slurry was washed with PBS, 10% glycerol, 5 mM DTT, pH 7.3. The fusion protein was cleaved with TEV protease (produced in-house) at 4°C overnight to remove the GST-tag. Resin was packed into a column while collecting protein in the flow-through. Protein eluting upon an additional wash step with buffer was combined with the flow-through. After a buffer exchange to 50 mM HEPES, 50 mM NaCl, 5 mM DTT, 5% glycerol, pH 7.3 on a HiPrep Desalting column (GE Healthcare) the protein was applied to cation- and anion-exchange columns coupled in series (Mono S(1^{st})-Mono Q(2^{nd}) (GE Healthcare)), pre-equilibrated with 50 mM HEPES, 50 mM NaCl, 5 mM DTT, 5% glycerol, pH 7.3. After separating the columns the recombinant protein was eluted from the Mono Q column by a gradient to 1 M NaCl. The eluted protein fraction was further purified on a gel filtration column (HiLoad Superdex S200, GE Healthcare) pre-equilibrated with 50 mM HEPES, 150 mM NaCl, 5 mM DTT, 5% glycerol, pH 7.3. The purified protein was concentrated to ~13 mg/ml and stored at -80 °C before further use.

The purified protein was incubated with a 2-fold molar excess of a K48 linked-ubiquitin dimer for 30 minutes and crystallized with the vapour diffusion method. 1 µL of protein solution (10.5 mg/mL in 50 mM HEPES, 50mM NaCl, 5% Glycerol, 5mM DTT pH 7,3) was mixed with 1 µL of reservoir solution containing 100 mM HEPES pH 6.0 and 0.95 M ammonium sulfate at 20 °C. Data were collected on an in-house Cu sealed tube (Rigaku MicroMax-003) and processed using AutoProc (Vonrhein et al., 2011). The structure was solved by sulphur-SAD and automatically built using the AutoSol wizard of Phenix (Adams et al., 2010). The autobuilt model contained 378 of the 448 residues present in the asymmetric unit and was further refined using COOT (Emsley et al., 2010) and AutoBUSTER (Bricogne et al., 2016). See Table S2 for data collection and refinement statistics.

Determination of membrane protein topology

Potential transmembrane regions of $USP35^{1-1018}$ were predicted using ΔG predictor (Hessa et al., 2007) and TMpred (http://www.ch.embnet.org/software/TMPRED_form.html).

Protease protection assay was carried out using U2OS FlpIn cells induced with 200 ng/ml tetracycline for 48h in order to express the indicated proteins. Cells from a 15-cm dish were trypsinised, spun down and resuspended in 4 ml ice-cold KHM buffer (20 mM HEPES-NaOH, pH 7.5, 110 mM KOAc, 2 mM $Mg(OAc)_2$). Digitonin was added to a final concentration of 80 μg/ml and samples incubated on ice for 5 min, at which point they were diluted to 14 ml with KHM buffer and cells spun down. Cells were resupended in 5 ml ice-cold HEPES buffer (90 mM HEPES-NaOH, pH 7.5, 50 mM KOAc), incubated for 10 min on ice and again isolated by centrifugation. Cells were resuspended in 1 ml ice-cold KHM buffer, counted and after pelleting resuspended in ice-cold KHM buffer. Proteolysis was carried out using equal number of cells expressing each construct in reactions supplemented with 0.5 mg/ml trypsin or 0.1 mM HCl used as a control. Reactions were performed for 1h on ice, stopped by the addition of soybean trypsin inhibitor (final concentration 1.25 mg/ml) and incubated for additional 10 min on ice. Sample buffer was added and samples denatured by heating at 70°C, for 10 min.

In order to determine the topology using N-glycosylation as a read-out U2OS FlpIn cells transfected with USP35 constructs tagged with a peptide derived from bovine rhodopsin (SRMNGTEGPNFYVPFSNKTVD) were lysed and denatured in SDS sample buffer at 70°C for 10 min. 500 U of Endoglycosidase H (EndoH) was added and samples incubated for 5h at 37°C.

Subcellular fractionation

Cells were washed with PBS, harvested and cell pellets resuspended in hypotonic buffer (10 mM HEPES-NaOH, pH 7.5, 1.5 mM $Mg(OAc)_2$, 10 mM KOAc, 0.5 mM DTT) supplemented with 1 mM AEBSF and complete protease inhibitor cocktail. After 10 min incubation on ice, cells were lysed by passing 10 times through a 27G needle. Cell debris and nuclei were pelleted by centrifugation (1000 x g, 10 min, 4°C) yielding a post-nuclear supernatant. Cytosolic and membrane fractions were separated by ultracentrifugation at 100,000 x g, 15 min, 4°C.

Proliferation assay

U2OS FlpIn cell lines were seeded in full DMEM medium into a 96-well plate at 5 000 cells/well (in total volume of 100 μl/well) and the next day protein expression was induced with 200 ng/ml tetracycline. Non-induced cells were analysed in parallel and each condition

was replicated in three separate wells. After 48h incubation 20 µl of the 3-(4,5-dimethylthiazol-2-yl)-5-(3-carboxymethoxyphenyl)-2-(4-sulfophenyl)-2H-tetrazolium, inner salt (MTS) reagent (Promega) was added and plates incubated for 90 min in a humidified incubator at 37°C. Absorbance was measured at 490 nm and the values obtained for media only were used as controls and subtracted from the results obtained for the samples analysed. Results were processed with Microsoft Excel software and graphs prepared with Prism 7 software. Three biological replicates were carried out. The same assay was used to estimate the viability of HEK293 FlpIn parental and knock-out clones in response to TRAIL treatment but cells were grown in DMEM without phenol red.

Immunoprecipitation

HeLa cells were treated with 1 µM staurosporine for the times shown in the presence of 20 µM zVAD-fmk where indicated. Cell pellets were resuspended in buffer A (20 mM HEPES-NaOH, pH 7.5, 110 mM KOAc, 2 mM $Mg(OAc)_2$, 1 mM EGTA, 0.1% (w/v) NP-40) supplemented with 1 mM Na_3VO_4, 1 mM NaF, 25 mM iodoacetamide, 1 mM AEBSF and complete protease inhibitor cocktail. Samples were incubated for 30 min on ice followed by two rounds of snap freezing in liquid N_2 and thawing at 30°C. Insoluble material was pelleted by centrifugation (16000 x g, 30 min, 4°C) and NaCl concentration adjusted to 150 mM. After pre-clearing with Protein G Agarose soluble fraction was subjected to immunoprecipitation with anti-USP35 antibodies or GFP trap resin (ChromoTek) for 2h at 4°C. Beads were washed three times with buffer A supplemented with 150 mM NaCl, resuspended in SDS sample buffer and proteins denatured for 10 min at 70°C. For USP35 immunoprecipitation from HPAF-II cells samples were processed as described above but cells were lysed in RIPA buffer (50 mM Tris-Cl, pH 7.5, 150 mM NaCl, 1% (w/v) NP-40, 0.5% (w/v) sodium deoxycholate, 0.1% (w/v) SDS) supplemented with 1 mM AEBSF, complete protease inhibitor cocktail and 0.1% benzonase.

BioID

BioID experiment was carried out essentially as described by (Coyaud et al., 2015) with slight modifications. Briefly, $BirA^{R118G}$ (BirA*) was fused to the C-terminus of human $USP35^{iso1}$ and $USP35^{iso2}$ in pcDNA5 FRT/TO and stable HEK293 FlpIn cell lines were generated. Experiments were performed with 4 x 150 cm^2 dishes and expression was induced at ~60% confluency with 1µg/ml tetracycline (Sigma) for 24 h. Media was then replaced with

a fresh one supplemented with 50 µM biotin (Sigma) and cells were further incubated for 10 h. Cells were washed twice with PBS, scraped, cell pellets snap frozen in liquid nitrogen and stored at -80°C.

Cell pellets were lysed in 1 mL of modified RIPA lysis buffer (1% (v/v) NP-40, 50 mM Tris–HCl, pH 7.5, 0.5% (w/v) sodium deoxycholate, 150 mM NaCl, 1 mM EDTA, 1 mM EGTA, 0.1% (w/v) SDS, 1:500 protease inhibitor cocktail (Sigma), with 250 U benzonase nuclease (Sigma)) in agitator for 1h at 4°C. The lysate was centrifuged for 30 min at 20,817 x g at 4°C and clarified supernatant incubated with 30 µl prewashed Streptavidin-Sepharose beads (GE Healthcare, catalog no. 17-5113-01) for 3 hr at 4°C. Beads were collected by centrifugation (400 x g, 2 min), washed twice with RIPA buffer (1 ml per wash), twice with TAP lysis buffer (50 mM HEPES-KOH, pH 8.0, 2 mM EDTA, 10% (v/v) glycerol, 100 mM KCl, 0.1% (v/v) NP-40), and four times with 50 mM ammonium bicarbonate (ABC; pH 8.0). Beads were then resuspended in 200 µl ammonium bicarbonate buffer and treated with 1µg of sequencing grade modified trypsin (Promega, V5113) for 12 h at 37°C with agitation. Additional 1 µg of trypsin was added after overnight digestion, samples were reduced with 5 µl of 10 mM DTT and alkylated with 5 µl of 10 mM IAA. The supernatant containing the tryptic peptides was collected, de-salted using C_{18} micro-spin columns (The Nest Group, Inc.) and vacuum centrifuged. Peptides were re-suspended in 20 µl of 0.1% formic acid and 5 µl were used per MS run.

In-gel digestion

Protein bands were excised from Coomassie Brilliant Blue-stained SDS-PAGE gel, washed twice with water and twice with 50% acetonitrile. Proteins were reduced and alkylated with 10 mM DTT and 55 mM iodoacetamide, respectively, in 100 mM ammonium bicarbonate and digested with 200 ng sequencing grade modified trypsin (Promega, V5113) for 14-16 h. Peptides were extracted twice with 50% acetonitrile and twice with 50% acetonitrile containing 2% formic acid and combined supernatants were dried using a Speedvac (Thermo Savant).

Mass spectrometry

The resulting peptides were analyzed by nano-Liquid chromatography (nLC, Dionex ultimate 3000) coupled to mass spectrometry (MS, LTQ-Orbitrap Velos; Thermo Finnigan). Peptides were loaded on a pre-column (Acclaim pepmap, C_{18}, 100Å, 100µm; Thermo) at 5 µl/min

flow rate and resolved on analytical column (Acclaim PepMap C_{18}, 2 µm, 100 Å, 75 µm x 50 cm), with 185 min gradient program, buffer B (90% acetonitrile, 3% DMSO, 0.08% formic acid (v/v)) and buffer A (2% acetonitrile, 3% DMSO, 0.1% formic acid, (v/v)) of buffer B ranging from 1 to 45%. Data was acquired in data dependent mode, a parent ion scan was performed in the Orbitrap, using a resolving power of 60000; at m/z 400. Simultaneously, CID was performed in ion trap activation time of 10 ms, with top 15 precursor ions. Protein identification was carried out using Sequest search algorithm against Uniprot database by selecting semi-tryptic enzymatic digestion option.

Protein identification

The MS raw files were searched using MaxQuant (version 1.5.8.3) (Cox and Mann, 2008), with the integrated Andromeda search engine. For the identification of peptides and proteins the UniProt human FASTA database (March 2015) was used with the FDR < 0.01. Oxidized methionine (M) and acetylation (protein N-term) were set as variable modifications and carbamidomethyl (C) as fixed modification. MaxQuant LFQ (Label free quanti- tation) was enabled with the stand 'match between runs'. The *bona fide* USP35 interacting proteins were identified with spectral counting as input for SAINTexpress (Significance Analysis of INTeractome) (Teo et al., 2014) with BFDR value of 2%. The resulting high confidence interacting proteins (HCIPs) were then subjected to DAVID enrichment analysis for cell compartment (Huang da et al., 2009).

Bioinformatics analysis

To analyse isoform expression in primary tumours, the TCGA transcript expression levels have been downloaded from UCSC Xena (http://xena.ucsc.edu/) version 2016-04-12. RNA-Seq reads were processed with the RSEM tool based on Gencode v23 transcript annotation. TPM expression values have been extracted from the RSEM result files and transformed to log2(tpm+0.001) values.

Expression of USP35 isoforms in selected cell lines was addressed by submitting the cell lines to Illumina Truseq RNA-Seq sequencing (poly-A selection) on an Illumina HiSeq instrument. Reads were processed with cufflinks version 2.0.2-foss-2015a with parameters -u --max-bundle-frags 10000000 --max-bundle-length 10000000 --no-effective-length-correction --compatible-hits-norm --max-frag-multihits 1. Ensembl v70 (hg19) gene annotation was used to determine the transcript expression levels. FPKM expression values were extracted from the cufflinks result files for all USP35 isoforms.

Accession code

Coordinates and structure factors have been deposited in the Protein Data Bank under accession code 5TXK.

ACKNOWLEDGEMENTS

We are extremely grateful for the excellent technical assistance that we received during the preparation of this manuscript. In particular, we would like to thank: Axel Knebel, James Hastie, Hilary McLauchlan and Samantha Raggett for the purification of USP35 proteins used for DUB assays and *in vitro* caspase cleavage reactions, Thomas Macartney for designing and preparing DNA constructs used to generate USP35 knock-out clones, Richard Ewan for help in preparing reagents during the initial stages of the project and Fiona Brown for purifying anti-USP35 antibodies. We are grateful to Stephen High (University of Manchester) for the gift of anti-rhodopsin antibody and help during the revision stage of this manuscript. We would like to thank all members of the Kulathu group for their help and comments received during the preparation of this manuscript.

COMPETING INTERESTS

The authors declare no competing or financial interests.

FUNDING

This work was supported by the Medical Research Council UK (MC_UU_12016/6 to Y.K.), European Research Council (677623 to Y.K.), the EMBO Young Investigator Programme (Y.K.), EMBO Installation Grant (3057 to N.L.B.M.), FCT Investigator Starting Grant from Fundação para a Ciência e Tecnologia (Portugal) (IF/00595/2014 to N.L.B.M.)), Tenovus Scotland (T16/24 to P.L.) and the pharmaceutical companies supporting the Division of Signal Transduction Therapy. Y.K. is a Lister Institute Prize Fellow.

DATA AVAILABILITY

The raw mass spectrometry data have been deposited in ProteomeXchange Consortium via the PRIDE repository (Vizcaino et al., 2014) with ID: PXD009286

Username: reviewer41567@ebi.ac.uk

Password: vhoA10om

REFERENCES

Adams, P. D., Afonine, P. V., Bunkoczi, G., Chen, V. B., Davis, I. W., Echols, N., Headd, J. J., Hung, L. W., Kapral, G. J., Grosse-Kunstleve, R. W. et al. (2010). PHENIX: a comprehensive Python-based system for macromolecular structure solution. *Acta Crystallogr D Biol Crystallogr* **66**, 213-21.

Adamus, G., Zam, Z. S., Arendt, A., Palczewski, K., McDowell, J. H. and Hargrave, P. A. (1991). Anti-rhodopsin monoclonal antibodies of defined specificity: characterization and application. *Vision Res* **31**, 17-31.

Axten, J. M., Medina, J. R., Feng, Y., Shu, A., Romeril, S. P., Grant, S. W., Li, W. H., Heerding, D. A., Minthorn, E., Mencken, T. et al. (2012). Discovery of 7-methyl-5-(1-{[3-(trifluoromethyl)phenyl]acetyl}-2,3-dihydro-1H-indol-5-yl)-7H-p yrrolo[2,3-d]pyrimidin-4-amine (GSK2606414), a potent and selective first-in-class inhibitor of protein kinase R (PKR)-like endoplasmic reticulum kinase (PERK). *J Med Chem* **55**, 7193-207.

Bago, R., Malik, N., Munson, M. J., Prescott, A. R., Davies, P., Sommer, E., Shpiro, N., Ward, R., Cross, D., Ganley, I. G. et al. (2014). Characterization of VPS34-IN1, a selective inhibitor of Vps34, reveals that the phosphatidylinositol 3-phosphate-binding SGK3 protein kinase is a downstream target of class III phosphoinositide 3-kinase. *Biochem J* **463**, 413-27.

Bartke, T., Pohl, C., Pyrowolakis, G. and Jentsch, S. (2004). Dual role of BRUCE as an antiapoptotic IAP and a chimeric E2/E3 ubiquitin ligase. *Mol Cell* **14**, 801-11.

Bersuker, K., Peterson, C. W. H., To, M., Sahl, S. J., Savikhin, V., Grossman, E. A., Nomura, D. K. and Olzmann, J. A. (2018). A Proximity Labeling Strategy Provides Insights into the Composition and Dynamics of Lipid Droplet Proteomes. *Dev Cell* **44**, 97-112.e7.

Bhattacharyya, S. N., Habermacher, R., Martine, U., Closs, E. I. and Filipowicz, W. (2006). Relief of microRNA-mediated translational repression in human cells subjected to stress. *Cell* **125**, 1111-24.

Borgese, N., Gazzoni, I., Barberi, M., Colombo, S. and Pedrazzini, E. (2001). Targeting of a tail-anchored protein to endoplasmic reticulum and mitochondrial outer membrane by independent but competing pathways. *Mol Biol Cell* **12**, 2482-96.

Bricogne, G., Blanc, E., Brandl, M., Flensburg, C., Keller, P., Paciorek, W., Roversi, P., Sharff, A., Smart, O. S., Vonrhein, C. et al. (2016). BUSTER version 2.11.7. Cambridge, United Kingdom: Global Phasing Ltd.

Bulbarelli, A., Sprocati, T., Barberi, M., Pedrazzini, E. and Borgese, N. (2002). Trafficking of tail-anchored proteins: transport from the endoplasmic reticulum to the plasma membrane and sorting between surface domains in polarised epithelial cells. *J Cell Sci* **115**, 1689-702.

Buljan, M., Chalancon, G., Eustermann, S., Wagner, G. P., Fuxreiter, M., Bateman, A. and Babu, M. M. (2012). Tissue-specific splicing of disordered segments that embed binding motifs rewires protein interaction networks. *Mol Cell* **46**, 871-83.

Chin, S. F., Teschendorff, A. E., Marioni, J. C., Wang, Y., Barbosa-Morais, N. L., Thorne, N. P., Costa, J. L., Pinder, S. E., van de Wiel, M. A., Green, A. R. et al. (2007). High-resolution aCGH and expression profiling identifies a novel genomic subtype of ER negative breast cancer. *Genome Biol* **8**, R215.

Clague, M. J., Heride, C. and Urbe, S. (2015). The demographics of the ubiquitin system. *Trends Cell Biol* **25**, 417-26.

Conti, B. J., Elferich, J., Yang, Z., Shinde, U. and Skach, W. R. (2014). Cotranslational folding inhibits translocation from within the ribosome-Sec61 translocon complex. *Nat Struct Mol Biol* **21**, 228-35.

Cox, J. and Mann, M. (2008). MaxQuant enables high peptide identification rates, individualized p.p.b.-range mass accuracies and proteome-wide protein quantification. *Nat Biotechnol* **26**, 1367-72.

Coyaud, E., Mis, M., Laurent, E. M., Dunham, W. H., Couzens, A. L., Robitaille, M., Gingras, A. C., Angers, S. and Raught, B. (2015). BioID-based Identification of Skp Cullin F-box (SCF)beta-TrCP1/2 E3 Ligase Substrates. *Mol Cell Proteomics* **14**, 1781-95.

Denzer, A. J., Nabholz, C. E. and Spiess, M. (1995). Transmembrane orientation of signal-anchor proteins is affected by the folding state but not the size of the N-terminal domain. *Embo j* **14**, 6311-7.

Eastman, S. W., Yassaee, M. and Bieniasz, P. D. (2009). A role for ubiquitin ligases and Spartin/SPG20 in lipid droplet turnover. *J Cell Biol* **184**, 881-94.

Ellis, J. D., Barrios-Rodiles, M., Colak, R., Irimia, M., Kim, T., Calarco, J. A., Wang, X., Pan, Q., O'Hanlon, D., Kim, P. M. et al. (2012). Tissue-specific alternative splicing remodels protein-protein interaction networks. *Mol Cell* **46**, 884-92.

Emsley, P., Lohkamp, B., Scott, W. G. and Cowtan, K. (2010). Features and development of Coot. *Acta Crystallogr D Biol Crystallogr* **66**, 486-501.

Engel, K., Rudelius, M., Slawska, J., Jacobs, L., Ahangarian Abhari, B., Altmann, B., Kurutz, J., Rathakrishnan, A., Fernandez-Saiz, V., Brunner, A. et al. (2016). USP9X stabilizes XIAP to regulate mitotic cell death and chemoresistance in aggressive B-cell lymphoma. *EMBO Mol Med* **8**, 851-62.

Faesen, A. C., Luna-Vargas, M. P., Geurink, P. P., Clerici, M., Merkx, R., van Dijk, W. J., Hameed, D. S., El Oualid, F., Ovaa, H. and Sixma, T. K. (2011). The differential modulation of USP activity by internal regulatory domains, interactors and eight ubiquitin chain types. *Chem Biol* **18**, 1550-61.

Floor, S. N. and Doudna, J. A. (2016). Tunable protein synthesis by transcript isoforms in human cells. *Elife* **5**.

Glab, J. A., Doerflinger, M., Nedeva, C., Jose, I., Mbogo, G. W., Paton, J. C., Paton, A. W., Kueh, A. J., Herold, M. J., Huang, D. C. et al. (2017). DR5 and caspase-8 are dispensable in ER stress-induced apoptosis. *Cell Death Differ* **24**, 944-950.

Han, S., Lone, M. A., Schneiter, R. and Chang, A. (2010). Orm1 and Orm2 are conserved endoplasmic reticulum membrane proteins regulating lipid homeostasis and protein quality control. *Proc Natl Acad Sci U S A* **107**, 5851-6.

Hao, Y., Sekine, K., Kawabata, A., Nakamura, H., Ishioka, T., Ohata, H., Katayama, R., Hashimoto, C., Zhang, X., Noda, T. et al. (2004). Apollon ubiquitinates SMAC and caspase-9, and has an essential cytoprotection function. *Nat Cell Biol* **6**, 849-60.

Hassink, G. C., Zhao, B., Sompallae, R., Altun, M., Gastaldello, S., Zinin, N. V., Masucci, M. G. and Lindsten, K. (2009). The ER-resident ubiquitin-specific protease 19 participates in the UPR and rescues ERAD substrates. *EMBO Rep* **10**, 755-61.

Heideker, J. and Wertz, I. E. (2015). DUBs, the regulation of cell identity and disease. *Biochem J* **465**, 1-26.

Hershko, A. and Ciechanover, A. (1998). The ubiquitin system. *Annu Rev Biochem* **67**, 425-79.

Hessa, T., Meindl-Beinker, N. M., Bernsel, A., Kim, H., Sato, Y., Lerch-Bader, M., Nilsson, I., White, S. H. and von Heijne, G. (2007). Molecular code for transmembrane-helix recognition by the Sec61 translocon. *Nature* **450**, 1026-30.

Hornle, M., Peters, N., Thayaparasingham, B., Vorsmann, H., Kashkar, H. and Kulms, D. (2011). Caspase-3 cleaves XIAP in a positive feedback loop to sensitize melanoma cells to TRAIL-induced apoptosis. *Oncogene* **30**, 575-87.

Huang da, W., Sherman, B. T. and Lempicki, R. A. (2009). Systematic and integrative analysis of large gene lists using DAVID bioinformatics resources. *Nat Protoc* **4**, 44-57.

Jeong, M., Lee, E. W., Seong, D., Seo, J., Kim, J. H., Grootjans, S., Kim, S. Y., Vandenabeele, P. and Song, J. (2017). USP8 suppresses death receptor-mediated apoptosis by enhancing FLIPL stability. *Oncogene* **36**, 458-470.

Kim, W., Bennett, E. J., Huttlin, E. L., Guo, A., Li, J., Possemato, A., Sowa, M. E., Rad, R., Rush, J., Comb, M. J. et al. (2011). Systematic and quantitative assessment of the ubiquitin-modified proteome. *Mol Cell* **44**, 325-40.

Klemm, E. J., Spooner, E. and Ploegh, H. L. (2011). Dual role of ancient ubiquitous protein 1 (AUP1) in lipid droplet accumulation and endoplasmic reticulum (ER) protein quality control. *J Biol Chem* **286**, 37602-14.

Lee, E. W., Seong, D., Seo, J., Jeong, M., Lee, H. K. and Song, J. (2015). USP11-dependent selective cIAP2 deubiquitylation and stabilization determine sensitivity to Smac mimetics. *Cell Death Differ* **22**, 1463-76.

Lee, J. G., Takahama, S., Zhang, G., Tomarev, S. I. and Ye, Y. (2016). Unconventional secretion of misfolded proteins promotes adaptation to proteasome dysfunction in mammalian cells. *Nat Cell Biol* **18**, 765-76.

Leznicki, P., Clancy, A., Schwappach, B. and High, S. (2010). Bat3 promotes the membrane integration of tail-anchored proteins. *J Cell Sci* **123**, 2170-8.

Leznicki, P. and Kulathu, Y. (2017). Mechanisms of regulation and diversification of deubiquitylating enzyme function. *J Cell Sci* **130**, 1997-2006.

Liu, C., Wang, L., Chen, W., Zhao, S., Yin, C., Lin, Y., Jiang, A. and Zhang, P. (2015). USP35 activated by miR let-7a inhibits cell proliferation and NF-kappaB activation through stabilization of ABIN-2. *Oncotarget* **6**, 27891-906.

Lu, M., Lawrence, D. A., Marsters, S., Acosta-Alvear, D., Kimmig, P., Mendez, A. S., Paton, A. W., Paton, J. C., Walter, P. and Ashkenazi, A. (2014). Opposing unfolded-protein-response signals converge on death receptor 5 to control apoptosis. *Science* **345**, 98-101.

Maatta, J., Hallikas, O., Welti, S., Hilden, P., Schroder, J. and Kuismanen, E. (2000). Limited caspase cleavage of human BAP31. *FEBS Lett* **484**, 202-6.

Mahul-Mellier, A. L., Pazarentzos, E., Datler, C., Iwasawa, R., AbuAli, G., Lin, B. and Grimm, S. (2012). De-ubiquitinating protease USP2a targets RIP1 and TRAF2 to mediate cell death by TNF. *Cell Death Differ* **19**, 891-9.

Mei, Y., Hahn, A. A., Hu, S. and Yang, X. (2011). The USP19 deubiquitinase regulates the stability of c-IAP1 and c-IAP2. *J Biol Chem* **286**, 35380-7.

Ng, F. W., Nguyen, M., Kwan, T., Branton, P. E., Nicholson, D. W., Cromlish, J. A. and Shore, G. C. (1997). p28 Bap31, a Bcl-2/Bcl-XL- and procaspase-8-associated protein in the endoplasmic reticulum. *J Cell Biol* **139**, 327-38.

Park, J., Kwon, M. S., Kim, E. E., Lee, H. and Song, E. J. (2018). USP35 regulates mitotic progression by modulating the stability of Aurora B. *Nat Commun* **9**, 688.

Pineau, L., Colas, J., Dupont, S., Beney, L., Fleurat-Lessard, P., Berjeaud, J. M., Berges, T. and Ferreira, T. (2009). Lipid-induced ER stress: synergistic effects of sterols and saturated fatty acids. *Traffic* **10**, 673-90.

Pohl, C. and Jentsch, S. (2008). Final stages of cytokinesis and midbody ring formation are controlled by BRUCE. *Cell* **132**, 832-45.

Popovic, D., Vucic, D. and Dikic, I. (2014). Ubiquitination in disease pathogenesis and treatment. *Nat Med* **20**, 1242-53.

Promlek, T., Ishiwata-Kimata, Y., Shido, M., Sakuramoto, M., Kohno, K. and Kimata, Y. (2011). Membrane aberrancy and unfolded proteins activate the endoplasmic reticulum stress sensor Ire1 in different ways. *Mol Biol Cell* **22**, 3520-32.

Rojas-Rivera, D., Delvaeye, T., Roelandt, R., Nerinckx, W., Augustyns, K., Vandenabeele, P. and Bertrand, M. J. M. (2017). When PERK inhibitors turn out to be new potent RIPK1 inhibitors: critical issues on the specificity and use of GSK2606414 and GSK2656157. *Cell Death Differ* **24**, 1100-1110.

Roux, K. J., Kim, D. I., Raida, M. and Burke, B. (2012). A promiscuous biotin ligase fusion protein identifies proximal and interacting proteins in mammalian cells. *J Cell Biol* **196**, 801-10.

Schwickart, M., Huang, X., Lill, J. R., Liu, J., Ferrando, R., French, D. M., Maecker, H., O'Rourke, K., Bazan, F., Eastham-Anderson, J. et al. (2010). Deubiquitinase USP9X stabilizes MCL1 and promotes tumour cell survival. *Nature* **463**, 103-7.

Shao, S. and Hegde, R. S. (2011). Membrane protein insertion at the endoplasmic reticulum. *Annu Rev Cell Dev Biol* **27**, 25-56.

Shen, L., Dong, A., Hu, J., Li, Y., Tempel, W., Bountra, C., Arrowsmith, C. H., Edwards, A. M. and Tong, Y. Crystal Structure of the N-terminal Domain of Human Ubiquitin Specific Protease 38. .

Spandl, J., Lohmann, D., Kuerschner, L., Moessinger, C. and Thiele, C. (2011). Ancient ubiquitous protein 1 (AUP1) localizes to lipid droplets and binds the E2 ubiquitin conjugase G2 (Ube2g2) via its G2 binding region. *J Biol Chem* **286**, 5599-606.

Tabas, I. and Ron, D. (2011). Integrating the mechanisms of apoptosis induced by endoplasmic reticulum stress. *Nat Cell Biol* **13**, 184-90.

Teo, G., Liu, G., Zhang, J., Nesvizhskii, A. I., Gingras, A. C. and Choi, H. (2014). SAINTexpress: improvements and additional features in Significance Analysis of INTeractome software. *J Proteomics* **100**, 37-43.

Thibault, G., Shui, G., Kim, W., McAlister, G. C., Ismail, N., Gygi, S. P., Wenk, M. R. and Ng, D. T. (2012). The membrane stress response buffers lethal effects of lipid disequilibrium by reprogramming the protein homeostasis network. *Mol Cell* **48**, 16-27.

Udeshi, N. D., Svinkina, T., Mertins, P., Kuhn, E., Mani, D. R., Qiao, J. W. and Carr, S. A. (2013). Refined preparation and use of anti-diglycine remnant (K-epsilon-GG) antibody enables routine quantification of 10,000s of ubiquitination sites in single proteomics experiments. *Mol Cell Proteomics* **12**, 825-31.

Vizcaino, J. A., Deutsch, E. W., Wang, R., Csordas, A., Reisinger, F., Rios, D., Dianes, J. A., Sun, Z., Farrah, T., Bandeira, N. et al. (2014). ProteomeXchange provides globally coordinated proteomics data submission and dissemination. *Nat Biotechnol* **32**, 223-6.

Vonrhein, C., Flensburg, C., Keller, P., Sharff, A., Smart, O., Paciorek, W., Womack, T. and Bricogne, G. (2011). Data processing and analysis with the autoPROC toolbox. *Acta Crystallogr D Biol Crystallogr* **67**, 293-302.

Wang, Y., Serricchio, M., Jauregui, M., Shanbhag, R., Stoltz, T., Di Paolo, C. T., Kim, P. K. and McQuibban, G. A. (2015). Deubiquitinating enzymes regulate PARK2-mediated mitophagy. *Autophagy* **11**, 595-606.

Weber, A., Heinlein, M., Dengjel, J., Alber, C., Singh, P. K. and Hacker, G. (2016). The deubiquitinase Usp27x stabilizes the BH3-only protein Bim and enhances apoptosis. *EMBO Rep* **17**, 724-38.

Welte, M. A. (2015). Expanding roles for lipid droplets. *Curr Biol* **25**, R470-81.

Wilhelm, M., Schlegl, J., Hahne, H., Gholami, A. M., Lieberenz, M., Savitski, M. M., Ziegler, E., Butzmann, L., Gessulat, S., Marx, H. et al. (2014). Mass-spectrometry-based draft of the human proteome. *Nature* **509**, 582-7.

Yang, C. S., Sinenko, S. A., Thomenius, M. J., Robeson, A. C., Freel, C. D., Horn, S. R. and Kornbluth, S. (2014). The deubiquitinating enzyme DUBAI stabilizes DIAP1 to suppress Drosophila apoptosis. *Cell Death Differ* **21**, 604-11.

Yang, X., Coulombe-Huntington, J., Kang, S., Sheynkman, G. M., Hao, T., Richardson, A., Sun, S., Yang, F., Shen, Y. A., Murray, R. R. et al. (2016). Widespread Expansion of Protein Interaction Capabilities by Alternative Splicing. *Cell* **164**, 805-17.

Yau, R. and Rape, M. (2016). The increasing complexity of the ubiquitin code. *Nat Cell Biol* **18**, 579-86.

Ye, Y., Scheel, H., Hofmann, K. and Komander, D. (2009). Dissection of USP catalytic domains reveals five common insertion points. *Mol Biosyst* **5**, 1797-808.

Yin, J., Schoeffler, A. J., Wickliffe, K., Newton, K., Starovasnik, M. A., Dueber, E. C. and Harris, S. F. (2015). Structural Insights into WD-Repeat 48 Activation of Ubiquitin-Specific Protease 46. *Structure* **23**, 2043-54.

Zehmer, J. K., Bartz, R., Liu, P. and Anderson, R. G. (2008). Identification of a novel N-terminal hydrophobic sequence that targets proteins to lipid droplets. *J Cell Sci* **121**, 1852-60.

FIGURE LEGENDS

Figure 1. USP35 is an active, promiscuous DUB.

A. (Left panel) Organisation of USP35 transcripts encoding isoforms presented in this study. Orange and grey boxes represent exons and non-coding regions, respectively. Exon numbers are given. (Right panel) Domain organisation of USP35 isoforms. The USP domain of USP35 is shown together with catalytic Cys450 and an unstructured insertion spanning residues 604-753. HEAT repeat motif predicted based on the crystal structure of the N-terminus of a related protein, USP38 (PDB: 4RXX), and protein regions used to generate anti-USP35 antibodies are indicated. Uniprot accession numbers of each isoform are shown on the left.

B. Purified, recombinant full-length human USP35 (375 nM) was incubated with tetraubiquitins of defined linkage types (733 nM) at 37°C for the indicated times. Reactions were resolved by SDS-PAGE followed by silver staining of the gel.

C. Crystal structure of the fragment of human USP35 (residues 423-944) lacking the insertion region (residues 604-753) and complexed with ubiquitin is presented. The subdomains thumb, palm and fingers are shown in wheat, light pink and yellow, respectively, whilst the non-covalently bound distal ubiquitin is in green. The dashed line has been used to show the disordered regions. The co-ordinated zinc can be seen as a black sphere in the finger subdomain. A potential binding site of proximal ubiquitin is indicated. Close up views show the catalytic centre and selected residues mediating USP35-ubiquitin interactions.

Figure 2. USP35 isoforms localise to distinct intracellular compartments.

A. U2OS FlpIn inducible cells expressing USP35 isoforms bearing a C-terminal GFP tag were fixed with paraformaldehyde (PFA) and stained with anti-GFP antibody. Protein localisation was examined by fluorescence microscopy.

B. As in (A) but samples were simultaneously stained with anti-GFP and anti-BAP31 ER marker antibodies.

C. U2OS FlpIn USP35^{iso2} cell line was left untreated or loaded with 0.3 mM oleic acid for 16h, at which point expression of iso2 was induced. Following an 8h incubation cells were

fixed with PFA and stained with LipidTox Deep Red. LipidTox staining and intrinsic GFP fluorescence was analysed by microscopy.

D. Expression of USP35$^{245-432}$ with a C-terminal GFP tag in stably transfected U2OS FlpIn cells was induced with tetracycline. Cells were fixed, stained with anti-GFP and anti-BAP31 antibodies, and samples analysed by immunofluorescence microscopy. Scale bar, 15 μm (panels A, B and D) and 5 μm (panel C).

Figure 3. USP35 isoform 2 is a novel integral membrane DUB.

A. Expression of the indicated variants of USP35 in U2OS FlpIn cells was induced with tetracycline, cells were semi-permeabilised with digitonin and trypsin or buffer control added. Samples were incubated for 1h on ice, resolved by SDS-PAGE and immunoblotted with anti-GFP antibody. Immunoblotting for calnexin (CNX) was used to validate the assay. Red dot indicates the protease-resistant USP35 fragment whilst the arrow marks a protein species most likely corresponding to high amount of trypsin used in the assay.

B. U2OS FlpIn cells were transfected with USP35^{iso2} tagged at the N- or C-terminus with a peptide derived from bovine rhodopsin (OPG) that contains two N-glycosylation sites. Cells were lysed, samples incubated with endoglycosidase H (EndoH) and resolved by SDS-PAGE. Results were visualised by immunoblotting with an anti-rhodopsin antibody. Numbers on the left indicate the number of N-glycans added to USP35^{iso2} whilst arrowheads an EndoH-sensitive truncated product of the N-terminally tagged iso2.

C. As in (B) but USP35 truncation spanning residues 270-432 was used. Numbers on the left indicate the number of N-glycans attached to the USP35 fragment.

D. As in (B) but the indicated truncations of USP35 bearing an N-terminal OPG tag were used. Note that iso2 corresponds to “270-end” variant. Red circles represent N-glycosylated species.

E. Experimentally validated topology of USP35^{iso2}. Amino acid sequence and conservation of the predicted transmembrane region is shown. “*” indicates fully conserved residues, “:” conserved residues of “strong groups” and “.” conserved residues of “weak groups” based on

ClustalX. The sequences used were as follows: NP_065849.1 (*H. sapiens*), NP_001170883.1 (*M. musculus*), XP_015136357.1 (*G. gallus*), XP_002936594.2 (*X. tropicalis*) and NP_725167.1 (*D. melanogaster*).

F. HPAF-II cells were lysed in the absence of detergent, post-nuclear supernatant (PNS), cytosolic and membrane fractions isolated and endogenous USP35 identified by immunoblotting using anti-USP35 antibody raised against the extreme C-terminus of the protein. Lysates of HPAF-II cells transfected with untagged USP35 isoforms 1 and 2 were used as markers for the electrophoretic migration of USP35 isoforms. Calnexin (CNX) and tubulin were used as markers for the membrane and cytosolic fractions, respectively.

G. HPAF-II cells were lysed in RIPA buffer and USP35 immunoprecipitated using the indicated antibodies. Samples were resolved by SDS-PAGE and immunoblotted with anti-USP35 antibody recognising the C-terminal region of the protein. Ectopically expressed, untagged USP35 isoforms were used as markers for the electrophoretic mobility.

Figure 4. USP35 isoform 2 overexpression induces ER stress and apoptosis.

A. Expression of USP35^{iso2} tagged at the C-terminus with GFP was induced in U2OS FlpIn cells with tetracycline for 48h. Cells were fixed with PFA, co-stained with anti-GFP, anti-BAP31 and anti-SPP (signal peptide peptidase) antibodies and analysed by microscopy. Scale bar, 15 μm.

B. Expression of USP35^{iso2} or a control ER-localised construct GFP-b5 was initiated by adding tetracycline to U2OS FlpIn cell lines. After 48h cells were lysed, samples resolved by SDS-PAGE and immunoblotted using antibodies against the indicated proteins. cl. BAP31 – cleaved BAP31.

C. As in (B) but the cell lines were seeded into a 96-well plate and 48h post-induction MTS proliferation assay was performed. The values on the Y axis represent the ratio of absorbance read for induced to non-induced cells. Statistical significance was calculated using a one-way Anova test. Error bars indicate standard errors of mean with N=3 biological replicates, ****P<0.0001, ***P = 0.0002.

D. USP35^{iso2} tagged at the C-terminus with GFP was expressed in inducible U2OS FlpIn cell line for 24h in the presence of 5 μM GSK2606414 or DMSO control. Cells were lysed, samples resolved by SDS-PAGE and immunoblotted using antibodies against the indicated proteins.

E. As in (B) but HeLa FlpIn cell lines induced to express GFP-b5 or USP35^{iso2} were used.

F. Expression of USP35^{iso2} bearing a C-terminal GFP tag was induced in U2OS FlpIn cell line. Levels of the GFP-tagged protein and upregulation of BiP were monitored at the indicated time points by immunoblotting cell lysates with antibodies against the indicated proteins.

G. As in (B) but U2OS FlpIn cells stably transfected with GFP-USP19 were used as a control. "++" indicates higher concentration of tetracycline used for GFP-USP19 expression.

Figure 5. Inhibition of cholesterol biosynthesis blocks USP35^{iso2} induced ER stress.

A. U2OS FlpIn parental cells were pretreated with 10 μM mevastatin or lovastatin for 2h and incubated with 100 nM thapsigargin for additional 18h (lanes 2-4). In parallel, U2OS FlpIn cells were induced to express USP35^{iso2} for 48h in the presence of 10 μM statins. Samples were analysed as in Fig 4B. Control samples represent cells without thapsigargin treatment or USP35^{iso2} induction.

B. Samples after statin treatment and USP35^{iso2} induction as shown in (A, lanes 6-9) were analysed by quantitative Western blotting and fold change of BiP induction relative to control plotted. Statistical significance was calculated using a one-way Anova test. Error bars indicate standard errors of mean with N=3 biological replicates, ****P = 0.0001, NS, not significant.

C. As in Fig 4B but U2OS FlpIn cells expressing indicated variants of USP35^{iso2} in a tetracycline-inducible manner were used.

D. U2OS FlpIn cells expressing indicated variants of USP35^{iso2} for 24h were subjected to subcellular fractionation followed by Western blotting analysis.

E. U2OS FlpIn cells were induced to express indicated GFP-tagged variants of USP35^{iso2} or GFP-b5 for 24h. Cells were lysed, GFP-tagged proteins and their binding partners recovered and samples analysed by Western blotting against the indicated proteins.

F. Indicated USP35 fragments (numbering based on iso1) were tagged at the C-terminus with GFP and at the N-terminus with the first 61 residues of SPP encompassing its first transmembrane region (TM1). USP35^{iso2} and GFP fused to such N-terminal fragment of SPP served as controls. Cells were treated and samples processed as described for Fig 4B.

Figure 6. USP35 isoform 1 is an anti-apoptotic protein.

A. Expression of the indicated isoforms of USP35 in stably transfected U2OS FlpIn cell lines was carried out for 48h. Cells were lysed, samples resolved by SDS-PAGE and immunoblotted with antibodies against the indicated proteins. cl. BAP31 – cleaved BAP31.

B. HEK293 FlpIn stably transfected cell lines were induced to express FLAG-tagged USP35^{iso1} wild-type protein, its catalytically-inactive variant or empty vector control. 24h post-induction cells were treated with 50 ng/ml TRAIL. Cells were lysed, samples resolved by SDS-PAGE and processing of caspase-8 analysed by immunoblotting.

C. HEK293 FlpIn parental cell line and two USP35 knock-out clones were treated with 50 ng/ml TRAIL and samples were analysed as for (B).

D. As in (C) but the cell lines were seeded into a 96-well plate, incubated with 50 ng/ml TRAIL for the indicated times and MTS proliferation assay was performed. The values on the Y axis represent the ratio of absorbance read for treated to untreated cells. Error bars indicate standard errors of mean with N=3 biological replicates.

E. HEK293 FlpIn parental cell line and two USP35 knock-out clones were treated with increasing concentrations of staurosporine for 24h. Cells were lysed and samples analysed by immunoblotting with an antibody against cleaved caspase-3.

F. HeLa cells were transfected with wild-type USP35^{iso1} or a variant with Asp743 substituted for Ala, both tagged at the C-terminus with a GFP tag. 24h post-transfection 1 μM staurosporine was added and cells incubated for the indicated time. Cells were lysed, samples resolved by SDS-PAGE and analysed by immunoblotting against the indicated proteins.

Figure 7. Isoform-specific interactome of USP35.

A. HEK293 FlpIn cells expressing USP35^{iso1} or USP35^{iso2} tagged at their C-terminus with BirA^{R118G} were induced for 24h, biotinylated proteins recovered on Streptavidin Sepharose, identified by mass spectrometry and subjected to SAINT analysis and DAVID GO analysis. Green bars show GO terms for the percentage of genes identified whilst red line indicates -$\log_{10}$ p value.

B. Isoform-specific and shared interacting partners are shown.

A.

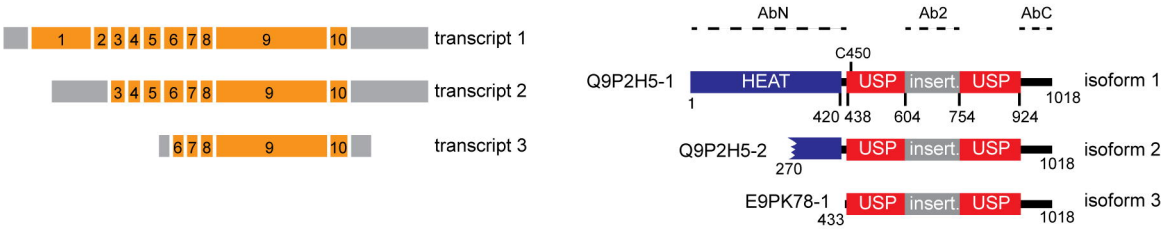
1 2 3 4 5 6 7 8 9 10
transcript 1
3 4 5 6 7 8 9 10
transcript 2
6 7 8 9 10
transcript 3
AbN
Ab2
AbC
C450
Q9P2H5-1
HEAT
USP
insert.
USP
isoform 1
1
420 438 604 754 924
1018
Q9P2H5-2
USP
insert.
USP
isoform 2
270
1018
E9PK78-1
USP
insert.
USP
isoform 3
433
1018

B.

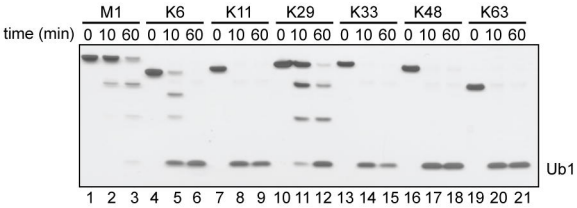
M1
K6
K11
K29
K33
K48
K63
time (min)
0 10 60 0 10 60 0 10 60 0 10 60 0 10 60 0 10 60 0 10 60
Ub1
1 2 3 4 5 6 7 8 9 10 11 12 13 14 15 16 17 18 19 20 21

C.

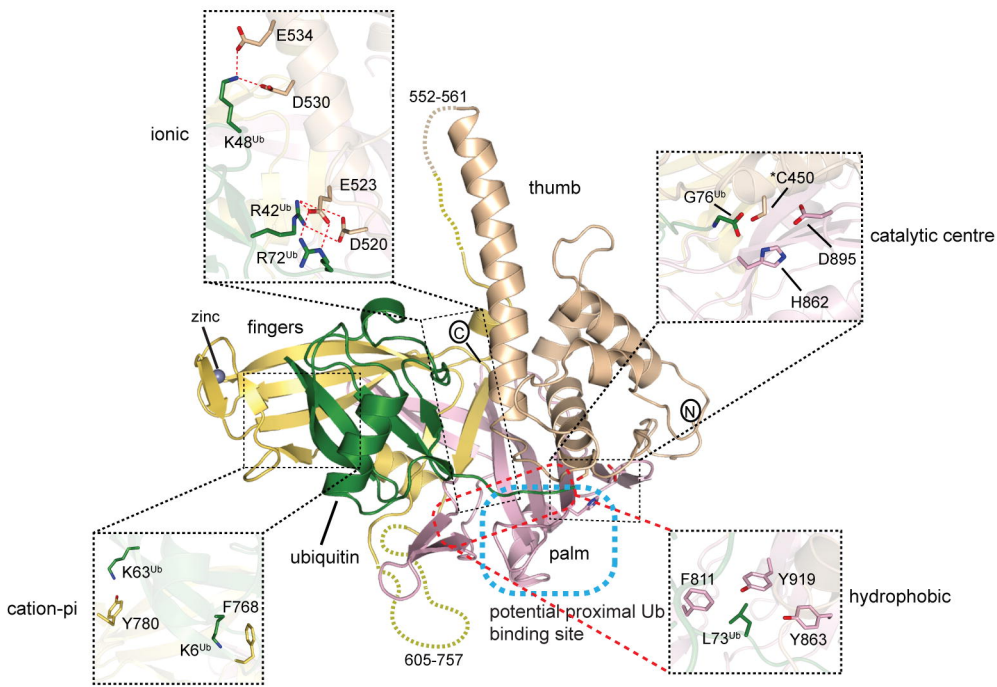
E534
D530
K48Ub
ionic
552-561
thumb
E523
R42Ub
D520
R72Ub
G76Ub
*C450
D895
H862
catalytic centre
zinc
fingers
C
N
ubiquitin
palm
K63Ub
cation-pi
Y780
F768
K6Ub
potential proximal Ub
binding site
605-757
F811
Y919
L73Ub
Y863
hydrophobic

A.

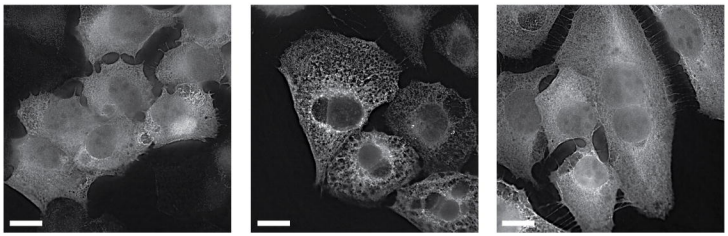

iso.1-GFP iso.2-GFP iso.3-GFP

B.

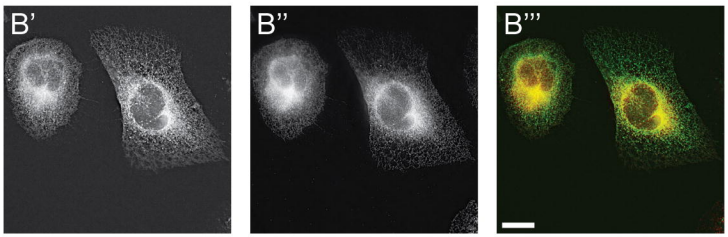

iso.2-GFP BAP31 merge

C.

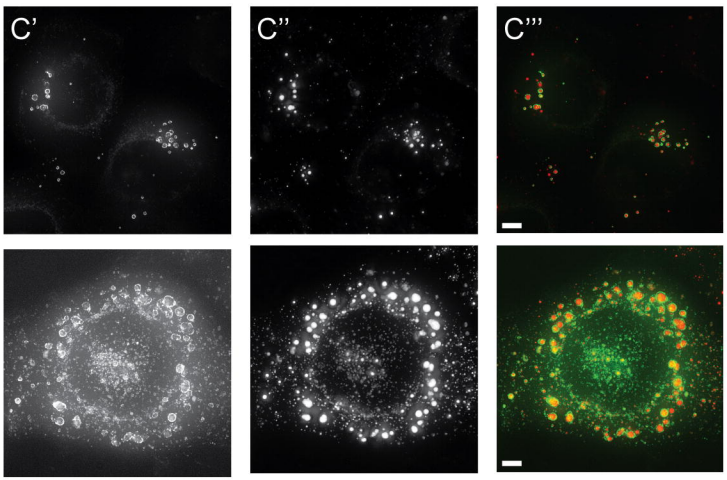

- oleic acid

+ oleic acid

iso.2-GFP LipidTox merge

D.

245-432-GFP BAP31 merge

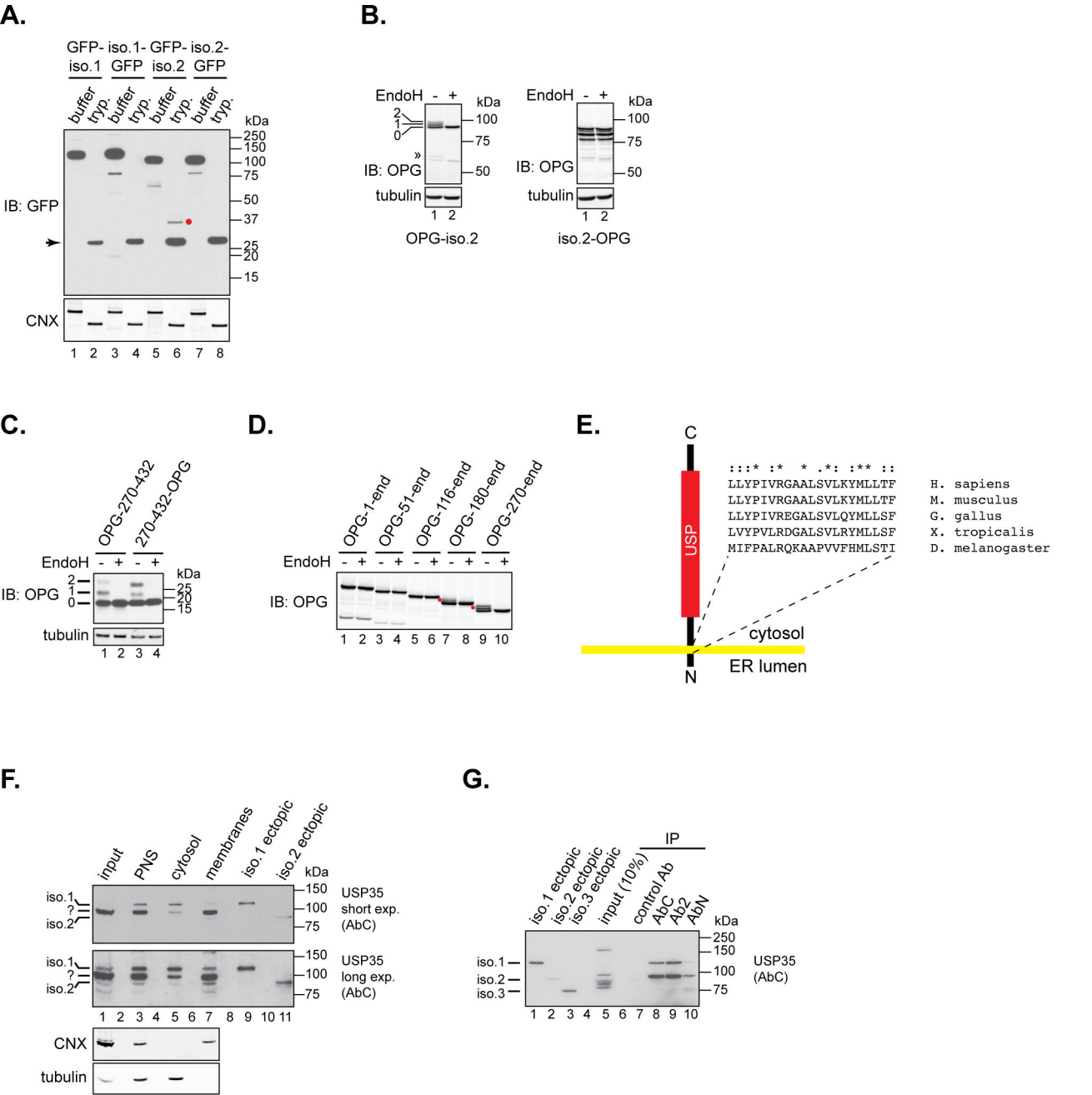
A.
GFP-iso.1
GFP-iso.2
buffer
tryp.
kDa
250
150
100
75
50
37
25
20
15
IB: GFP
CNX
1 2 3 4 5 6 7 8
B.
EndoH - +
kDa
100
75
50
IB: OPG
tubulin
1 2
OPG-iso.2
iso.2-OPG
C.
OPG-270-432
270-432-OPG
EndoH - + - +
IB: OPG
tubulin
1 2 3 4
D.
OPG-1-end
OPG-51-end
OPG-116-end
OPG-180-end
OPG-270-end
EndoH - + - + - + - + - +
IB: OPG
1 2 3 4 5 6 7 8 9 10
E.
C
USP
N
cytosol
ER lumen
::::* :* * .*: :** ::
LLYPIVRGAALSVLKYMLLTF H. sapiens
LLYPIVRGAALSVLKYMLLTF M. musculus
LLYPIVREGALSVLQYMLLSF G. gallus
LVYPVLRDGALSVLRYMLLSF X. tropicalis
MIFPALRQKAAPVVFHMLSTI D. melanogaster
F.
input
PNS
cytosol
membranes
iso.1 ectopic
iso.2 ectopic
kDa
iso.1
?
iso.2
150
100
75
USP35 short exp. (AbC)
USP35 long exp. (AbC)
1 2 3 4 5 6 7 8 9 10 11
CNX
tubulin
G.
iso.1 ectopic
iso.2 ectopic
iso.3 ectopic
input (10%)
IP
control Ab
AbC
Ab2
AbN
kDa
250
150
100
75
iso.1
iso.2
iso.3
USP35 (AbC)
1 2 3 4 5 6 7 8 9 10

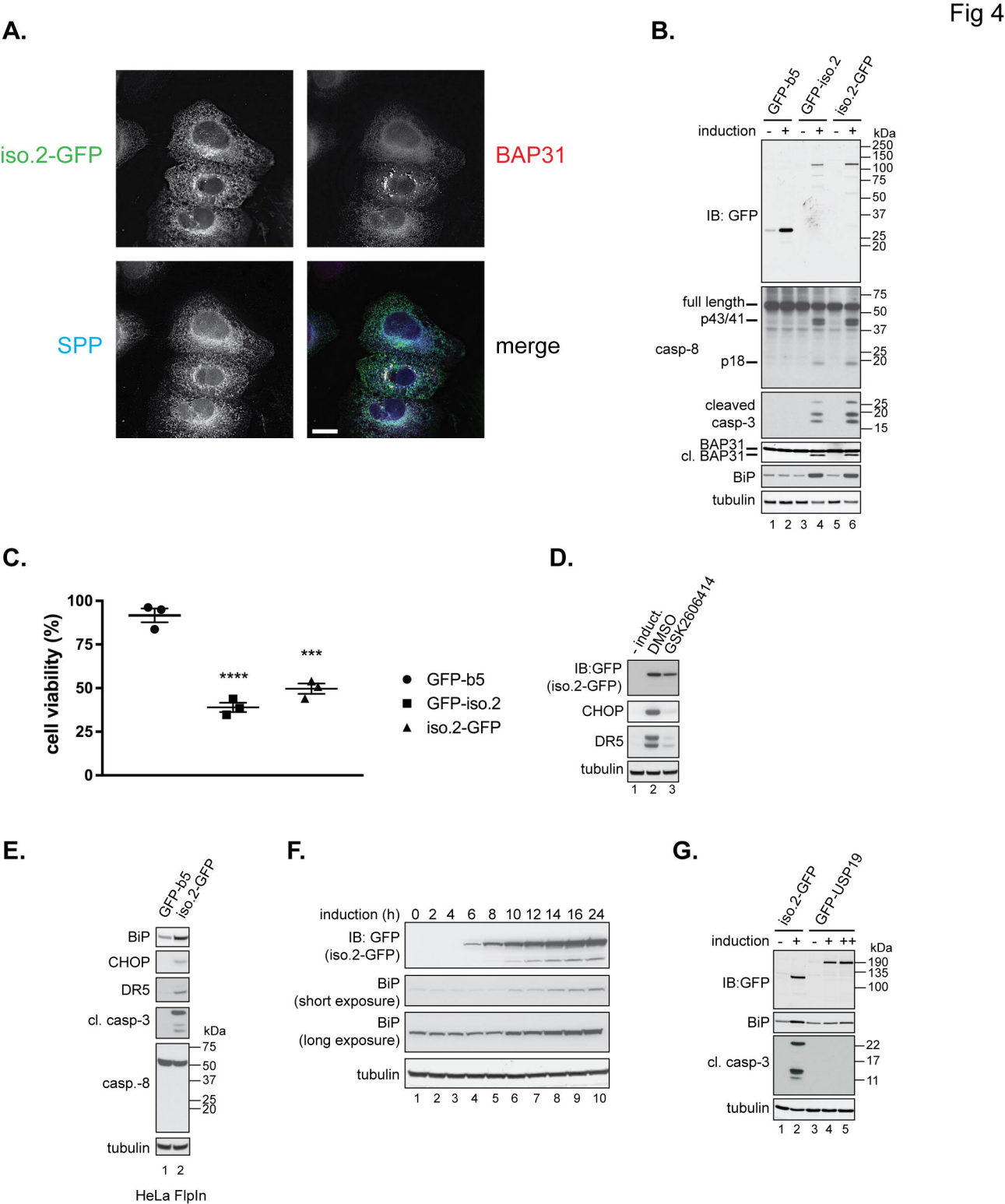
A.
iso.2-GFP
BAP31
SPP
merge
B.
GFP-b5
GFP-iso.2
iso.2-GFP
induction
kDa
IB: GFP
full length
p43/41
casp-8
p18
cleaved
casp-3
BAP31
cl. BAP31
BiP
tubulin
C.
cell viability (%)
GFP-b5
GFP-iso.2
iso.2-GFP
D.
- induct.
DMSO
GSK2606414
IB:GFP
(iso.2-GFP)
CHOP
DR5
tubulin
E.
BiP
CHOP
DR5
cl. casp-3
casp.-8
tubulin
HeLa FlpIn
F.
induction (h)
IB: GFP
(iso.2-GFP)
BiP
(short exposure)
BiP
(long exposure)
tubulin
G.
iso.2-GFP
GFP-USP19
induction
IB:GFP
BiP
cl. casp-3
tubulin

A.

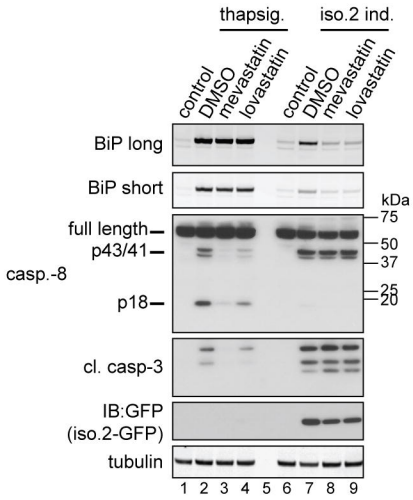
thapsig.
iso.2 ind.
control
DMSO
mevastatin
lovastatin
control
DMSO
mevastatin
lovastatin
BiP long
BiP short
full length
p43/41
casp.-8
p18
cl. casp-3
IB:GFP
(iso.2-GFP)
tubulin
kDa
75
50
37
25
20
1 2 3 4 5 6 7 8 9

B.

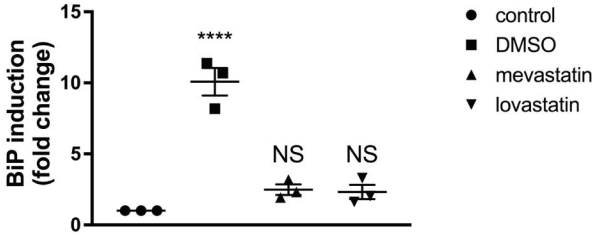
BiP induction
(fold change)
15
10
5
0
****
NS
NS
control
DMSO
mevastatin
lovastatin

C.

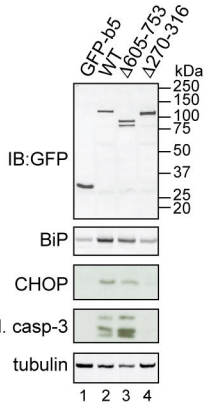
GFP-b5
WT
Δ605-753
Δ270-316
kDa
250
150
100
75
50
37
25
20
IB:GFP
BiP
CHOP
cl. casp-3
tubulin
1 2 3 4

D.

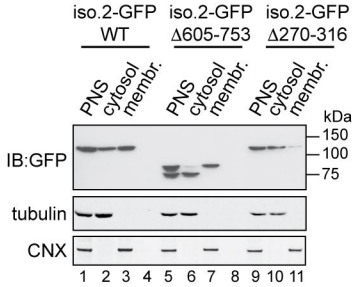
iso.2-GFP
WT
iso.2-GFP
Δ605-753
iso.2-GFP
Δ270-316
PNS
cytosol
membr.
PNS
cytosol
membr.
PNS
cytosol
membr.
kDa
150
100
75
IB:GFP
tubulin
CNX
1 2 3 4 5 6 7 8 9 10 11

E.

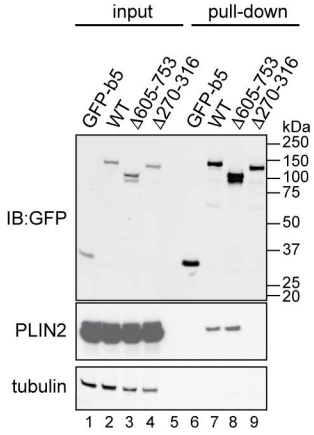
input
pull-down
GFP-b5
WT
Δ605-753
Δ270-316
GFP-b5
WT
Δ605-753
Δ270-316
kDa
250
150
100
75
50
37
25
20
IB:GFP
PLIN2
tubulin
1 2 3 4 5 6 7 8 9

F.

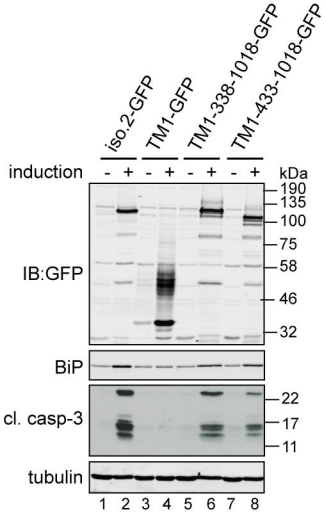
iso.2-GFP
TM1-GFP
TM1-338-1018-GFP
TM1-433-1018-GFP
induction
- + - + - + - +
kDa
190
135
100
75
58
46
32
22
17
11
IB:GFP
BiP
cl. casp-3
tubulin
1 2 3 4 5 6 7 8

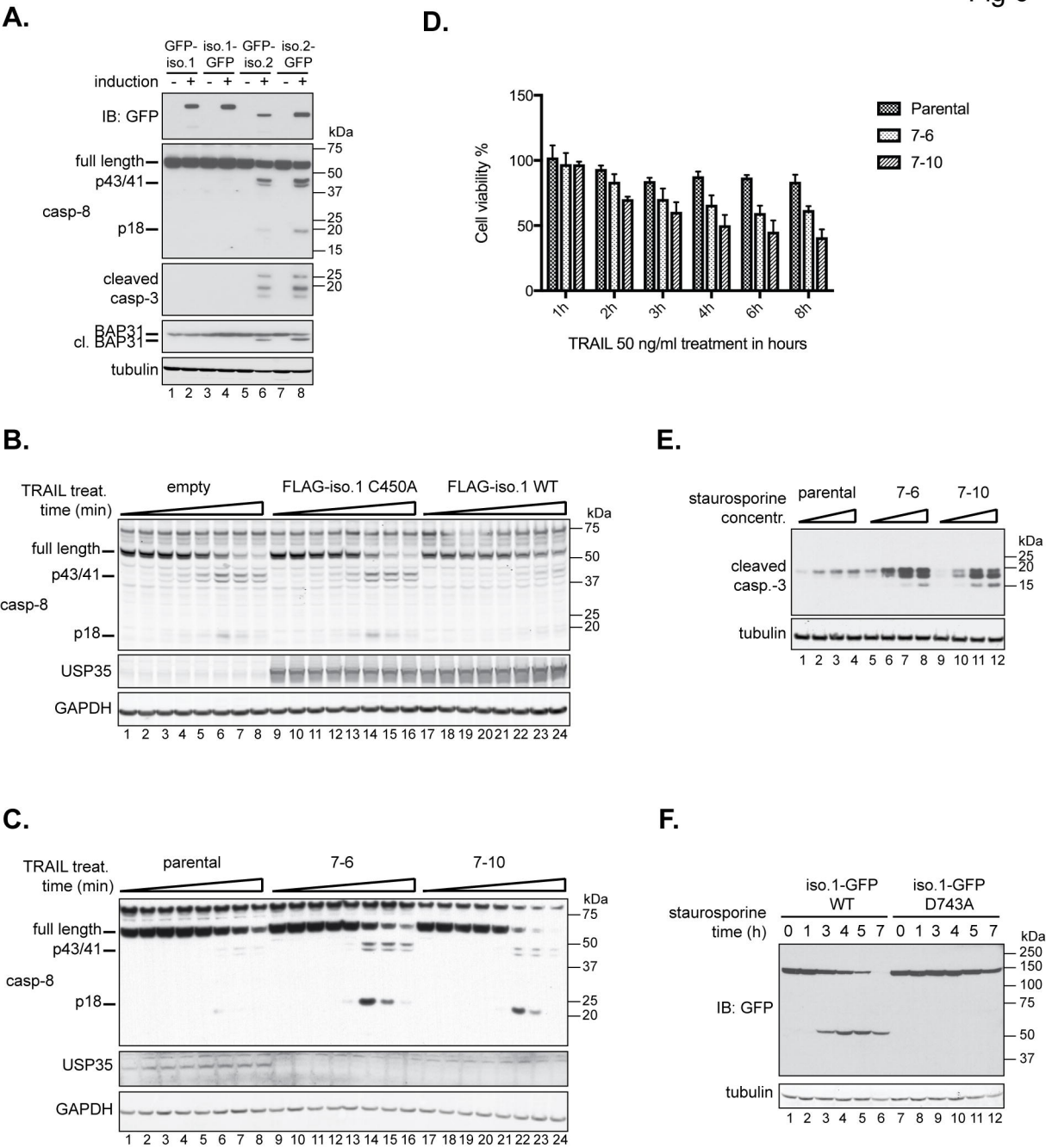
A.
GFP-iso.1
iso.1-GFP
GFP-iso.2
iso.2-GFP
induction - + - + - + - +
IB: GFP
kDa
75
full length
p43/41
50
37
casp-8
p18
25
20
15
cleaved casp-3
25
20
BAP31
cl. BAP31
tubulin
1 2 3 4 5 6 7 8
D.
150
100
50
0
Cell viability %
1h
2h
3h
4h
6h
8h
TRAIL 50 ng/ml treatment in hours
Parental
7-6
7-10
B.
TRAIL treat. time (min)
empty
FLAG-iso.1 C450A
FLAG-iso.1 WT
kDa
75
full length
p43/41
50
37
casp-8
p18
25
20
USP35
GAPDH
1 2 3 4 5 6 7 8 9 10 11 12 13 14 15 16 17 18 19 20 21 22 23 24
E.
staurosporine concentr.
parental
7-6
7-10
kDa
25
20
15
cleaved casp.-3
tubulin
1 2 3 4 5 6 7 8 9 10 11 12
C.
TRAIL treat. time (min)
parental
7-6
7-10
kDa
75
full length
p43/41
50
37
casp-8
p18
25
20
USP35
GAPDH
1 2 3 4 5 6 7 8 9 10 11 12 13 14 15 16 17 18 19 20 21 22 23 24
F.
staurosporine time (h)
iso.1-GFP WT
iso.1-GFP D743A
0 1 3 4 5 7 0 1 3 4 5 7
kDa
250
150
100
75
IB: GFP
50
37
tubulin
1 2 3 4 5 6 7 8 9 10 11 12

A.

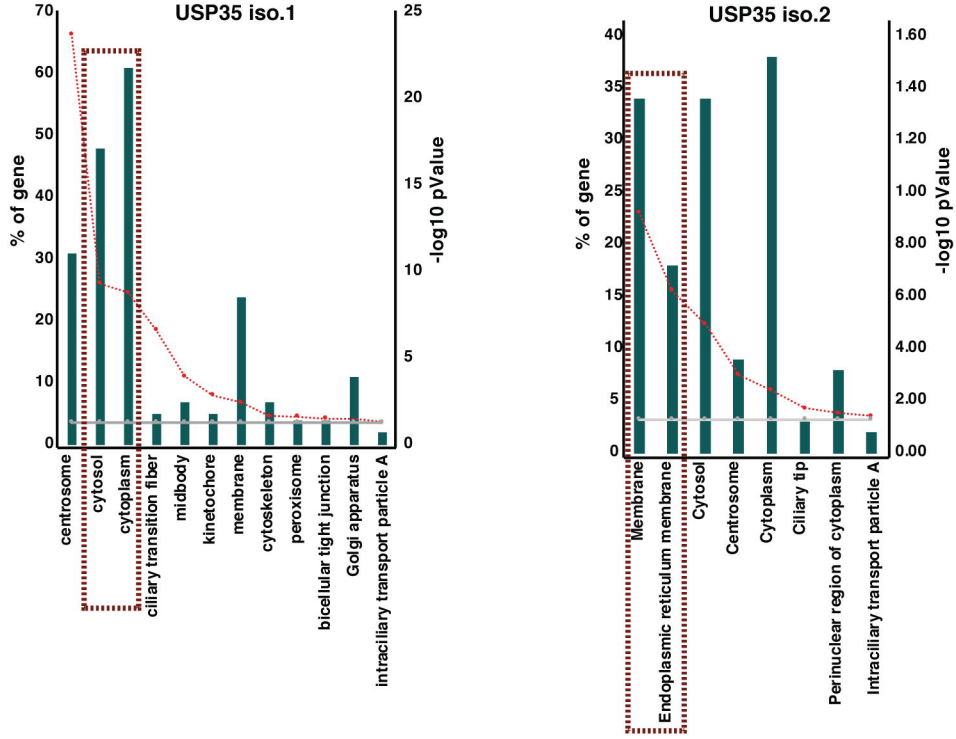

B.

USP35 iso.1					Shared proteins		USP35 iso.2		
UHRF1BP1L	PSMD7	RPGRIP1L	KIAA0232	AKAP11	TBKBP1	IFT140	NBAS	PDE3B	SNX19
WDR91	FAM193A	WWC2	SPAG5	PLEKHG1	RGPD8	CDK5RAP2	AIP	ITPR1	LRRC59
PIK3C2A	PPP2R3A	CEP85	PSMD1	HECTD1	NDC80	AKAP9	DEGS1	KIAA0100	MYO19
BACH1	FOXO1	PIK3AP1	MPHOSPH9	STUB1	PCNT	TCHP	FANCA	EMC2	SPG11
KIAA0355	TIAM1	USP54	PIK3R4	PDZRN3	HERC2	BBS2	EMC8	PLEC	KIF16B
PJA2	RABEP1	PHLDB2	RGPD5	ANKRD26	TBC1D8	BIRC6	ADCY9	CYP51A1	VPS13A
SIPA1L1	HERC1	AMOTL1	TSG101	CEP164	PI4KA	USP35	TRIM13	EDRF1	PKMYT1
FOXO3	MAPK6	ASPM	LZTS2	SSX2IP	CENPE	MAGED1	OBSL1	KLHL26	MTR
PEX1	KIF7	SPICE1	CEP295	GRIP1	GOLGA3		SKAP2	MIA3	NDC1
SIPA1L3	CCDC88A	CNTROB	RNF41	MTCL1	NCOA4		STBD1	DOCK11	C1orf43
PPP6R2	AMOT	NIN	C2orf44	NME7	ESPL1		HMGCR	RNFT1	DPH1
POLQ	PAN2	ANKRD52	CCSER2	PCLO	SPECC1		DNAJA1	SNAP47	ZYG11B
MPDZ	ARHGAP29	EHBP1	NCKAP5L		N4BP2		ABCC1	WLS	VEZT
SOGA1	WDR81	NAV1	ZNF277		IQGAP3		BAG6	CDKAL1	PREB
TRIM37	ODF2	PJA1	PCMTD2		BBS7		CAMLG	UBR3	STARD7
CEP152	CEP78	ALMS1	CNTLN		WDR19		TSC2	VRK2	AGPAT4
CLTA	CCDC18	RB1CC1	UBAP1		USP33		DNA2	FUK	SACS
AHR	MLK4	CEP192	CCDC88C		SYNE2		TTC3	TMEM57	CNOT8
PEX19	CEP350	DIS3L	SIPA1L2		NEURL4		SREBF2	DYNC2H1	HERC5
CENPF	PDE4DIP	IFT81	TBK1		EXOC2		BNIP1	PDZD8	FNDC3A
							UBE2J1		SNX14
50.5%					15.4%		34.1%		